Sandia National Laboratories

Operated for the United States Department of Energy
by National Technology and Engineering Solutions
of Sandia, LLC.
Albuquerque, New Mexico 87185-0747
Livermore, California 94551-0969

date: 9 March 2026

STEPHEN WAGNER (Affiliate) Digitally signed by STEPHEN WAGNER (Affiliate) Date: 2026.03.09 12:34:07 -06'00'

to: Steve Wagner, 8881
Ross Kirkes, 8881

from: Rob P. Rechard, 8844

subject: Fissile Mass and Concentration Necessary for Post-Closure Criticality in Geologic Media Near Bedded Salt Repository

ABSTRACT

This memorandum describes the fissile mass and concentration necessary for a critical event to occur in geologic media surrounding the Waste Isolation Pilot Plant (WIPP), an operating repository in southeastern New Mexico for disposing wastes containing transuranic (TRU) radioisotopes from atomic energy defense activities. In the past, concern about criticality in TRU waste has been low because of the low initial concentration of fissile material and the natural tendency of fissile solute to disperse during geologic transport. The potential disposal of TRU waste with high initial concentration of plutonium fissile material prompted a renewed evaluation of the criticality potential. The criticality limits are based on modeling mixtures of fissile plutonium and uranium with water, brine, salt, rust, clay, concrete, cellulose, sandstone, and dolomite in an idealized spherical geometry using neutron/photon transport codes. In most cases, materials are mixed homogeneously. Geologic media increases the necessary critical mass. Thus, the required critical mass is much larger than in water mixtures, especially for low enriched uranium. Understandably, decreasing the geologic porosity increases the critical mass but can cause the critical asymptotic concentration to decrease to that less than in water mixtures when the geologic media is a weak moderator. Brine fluids strongly increase both fissile mass and concentration critical limits. Fractured heterogeneous media is considered by developing a cell model of planar fractions in regular array to obtain equivalent neutron cross-section data. Spacing of fracture heterogeneity greatly influences fissile critical limits but fracture porosity has much less influence than matrix porosity. The criticality limits in geologic media are useful to demonstrate the low probability of criticality in radioactive disposal systems after closure when humans are absent.

Keywords: post-closure criticality evaluation; features, events, and processes screening; transuranic radioactive waste disposal; safety assessment; performance assessment; Waste Isolation Pilot Plant

Information Only

PREFACE

This memorandum presents results of neutron transport calculations of ideal spheres in porous homogeneous and fractured geologic media saturated with water or brines to roughly estimate minimum fissile masses and concentrations necessary for criticality in a geologic setting. These results by themselves do not determine whether criticality is possible within or outside a repository, such as the Waste Isolation Pilot Plant (WIPP) for transuranic waste from defense atomic energy activities. Rather, these results must be combined with an evaluation of the fissile masses and concentrations possible through mobilization and then deposition via precipitation, sorption, or colloid filtering (as presented in companion reports) to access the possibility of criticality during the 10 000-year regulatory period after WIPP closure. These calculations have been performed in accordance with the "reasonable expectation" standard of proof in the US Environmental Protection Agency (EPA) 40 CFR 191 Standard, as described in §191.13(b). Hence, this report is being issued outside of Sandia National Laboratories' Nuclear Criticality Safety Program that is governed under 10 CFR 830 and US Department of Energy (DOE) Order 420.1C, Chg. 3 without receiving that program's concurrence or dissension of the conclusions made within.

This 2025 memorandum updates the 2019 memorandum by R. P. Rechard, L. C. Sanchez, M. Olgvun, and G. Ryba, *Fissile Mass and Concentration Necessary for Criticality in Geologic Media near Bedded Salt Repository*, which supported the 2019 WIPP Compliance Recertification Application to EPA.

ACKNOWLEDGEMENTS

Phil Jones and Mariah Garcia of Sandia conducted the internal technical review. G. Ross Kirkes, Piru Associates, provided helpful insight on screening the post-closure criticality scenario. This memorandum would not have been possible without the dedication and efforts of Dr. Patrick J. McDaniel, Department of Nuclear Engineering, University of New Mexico, Albuquerque, New Mexico.

Information Only

CONTENTS

I. Introduction 9
II WIPP Disposal System 9
II.A Fissile Mass in TRU Waste 9
II.B. Geologic Characteristics of WIPP Disposal System 10
II.B.1. Salado Formation 10
II.B.2. Culebra Dolomite Member of Rustler Formation 11
I.B.3. Brine Compositions for Calculations 13
III. Calculation of Critical Concentration and Mass for Homogeneous Sphere 14
III.A. Computational Tools 14
III.A.1 SCALE 14
III.A.2 MCNP 15
III.B. Upper Subcriticality Limit and Bias 15
III.C. Critical Limits for Fissile-Fluid System 16
III.C.1 Plutonium-Fluid System 16
III.C.2. Uranium-Fluid System 17
III.D. Minor Influence of Deposited Mineral Form at High Enrichment 18
III.D.1. Mineral Forms of Plutonium 18
III.E.2. Mineral Forms of Uranium 19
III.E. Influence of Deposited Uranium Minerals at Low Enrichment 19
IV. Critical Limits for Homogeneous Sphere in Various Materials within Repository 19
IV.A. Critical Limits in Carbon-Rich Material 19
IV.A.1. Cellulose 19
IV.A.2. Polyethylene 20
IV.A.3. Pure Carbon and Water 20
IV.B. Critical Limits in Hydrated Clay 21
IV.C. Critical Limits in Iron 22
V. Critical Limits in Silicon-Rich Materials 23
V.A. Critical Limits in Cement/Concrete 23
V.B. Critical Limits in Sandstone 23
VI. Critical Limits in Evaporites 24
VI.A. Critical Limits in Halite and Halite/MgO Mixture 24
VI.B. Critical Limits in Homogeneous Culebra Dolomite 25
VII. Critical Limits Considering Heterogeneity in Culebra Dolomite 27
VII.A. Approach for Fracture Heterogeneity 27
VII.B. Plutonium in Culebra Fracture Array 28
VII.C. Uranium in Culebra Fracture Array 29
VII.D. Comparison with Heterogeneous Behavior in Volcanic Tuff 30
VII.D.1. Fracture System in Volcanic Tuff at Yucca Mountain 30
VII.D.2. Fracture System in Culebra Dolomite using Volcanic Tuff Fracture Parameters 31
VIII. Conclusions 32
VIII.A. Geologic Media Increases Critical Mass but often Decreases Critical Concentration 32
VIII.B. Brine Fluids Increase Critical Limits 33
VIII.C. Porosity Influences Critical Mass and Concentration 34
VIII.D. Fracture Spacing in Culebra Influences Critical Limits 34
VIII.E. Summary 35
References 37

Information Only

FIGURES

1. WIPP repository 42 km east of Carlsbad in the Delaware Basin in southeastern New Mexico.[1, Fig. 1] 9
2. Stratigraphic divisions of Culebra Dolomite Member of Rustler Formation.[38, Figure 3-6] 11
3. Upper subcriticality limit for critical mass for ^{235}U as UO_2 and UO_2CO_3 in Culebra dolomite with 20% and 30% porosity saturated with Culebra brine is non-linear at low enrichment.[10, Fig. 4] 15
4. Calculated and measured critical mass and radius as function of fissile concentration in a homogeneous, spherical shape in water and WIPP brines:[1, Fig. 5, 10, Fig. 5, 59, Fig. 7, 60, Fig. 27-1, 61] 16
5. Uranium calculated and measured critical concentration at various enrichments for a homogeneous, spherical shape in water.[10, Fig. 6, 59, Fig. 7, 60, 61] 17
6. Decrease of minimum critical concentration asymptote with increase in ^{239}Pu and ^{235}U enrichment in WIPP brines.[10, Fig. 7] 18
7. Pu and U mineral forms in Culebra dolomite/Culebra brine or volcanic tuff/fluid at 20% porosity.[10, Fig. 8] 18
8. Below 20% enrichment both Uranium mineral form and material matrix influences critical mass below 20% enrichment; only material matrix influences critical mass above 20% enrichment.[10, Fig. 9] 19
9. Critical limits of plutonium mixed with water, WIPP brines, and cellulose at various porosities. 20
10. Plutonium critical limits in polyethylene (100% and 74% volume), water (100% and 25%), Salado brine (100% and 25%), and beryllium (0 and 1%) with upper subcritical limit (USL) of unity and 0.938. 20
11. Plutonium critical limits in carbon with porosity between 5% and 80% filled with water and WIPP brines. 21
12. Critical limits for montmorillonite clay with ^{239}Pu or ^{235}U (5% enriched) at 20% to 40% porosity saturated with water or WIPP brine. 21
13. Critical limits of Pu in goethite (Fe rust) at 20% and 30% porosity filled with water and WIPP brines.[10, Fig. 13] 22
14. Critical limits of 93% and 5% enriched uranium in goethite (Fe rust) at 20% and 30% porosity filled with water and WIPP brines. [10, Fig. 13] 22
15. Critical limits of PuO_2 in NRC concrete and cement mixture with porosities between 10% and 20% filled with water or WIPP brine. [10, Fig. 17] 23
16. Critical limits in NRC concrete for 5% enriched $^{235}UO_2$ at porosities between 10% and 30% filled with water or WIPP brines. 23
17. Critical limits for 3.7% enriched UO_2 in sandstone at porosity from 15% to 45% filled with water.[10, Fig. 14] 24
18. Critical behavior for 100% enriched PuO_2 in sandstone at porosities between 10% and 45% filled with water. [10, Fig. 15] 24
19. Critical limits for PuO_2 in halite or halite/MgO matrix with porosity saturated with Salado brine.[10, Fig. 11] 25
20. Critical limits for PuO_2 in homogeneous Culebra dolomite with total porosity between 10% and 33% saturated with Culebra brine. [10, Fig. 18] 25
21. Critical limits for PuO_2 in homogeneous Culebra dolomite with total porosity between 10 % and 33% saturated with Castile brine. 26
22. Criticality limits for 5% enriched UO_2 in homogeneous Culebra dolomite with total porosity between 18% and 32% saturated with Culebra brine. [10, Fig. 19] 26
23. Critical limits of uranium as UO_2CO_3 and UO_2 at various enrichments in homogenous Culebra dolomite mostly at 23% total porosity saturated with Culebra brine. [10, Fig. 20] 26
24. Heterogeneous conceptual and computational models of fracture deposition in Culebra dolomite. [10, Fig. 22] 27
25. Critical limits of PuO_2 at variable matrix porosity ($\phi_{Culebra}^{mat+vug}$) with planar fractures saturated with Culebra brine for fracture spacing ($2B$) of 20 and 4 cm and fracture porosity (ϕ^{frac}) of 1% ($2b$ of 0.2 cm and 0.04 cm, respectively) 28
26. Critical limits of PuO_2 at variable $\phi_{Culebra}^{mat+vug}$ with planar fractures saturated with Castile brine for $2B$ of 20 and 4 cm and ϕ^{frac} of 1%. 28
27. Critical limits of 93% enriched UO_2 at variable $\phi_{Culebra}^{mat+vug}$ with planar fractures saturated with Culebra brine for $2B$ of 4 and 20 cm and ϕ^{frac} of 1%. 29
28. Critical limits of 93% enriched UO_2 at variable $\phi_{Culebra}^{mat+vug}$ with planar fractures saturated with Castile brine for $2B$ of 4 and 20 cm and ϕ^{frac} of 1% 29
29. Influence of fracture spacing on minimum critical mass of highly enriched ^{239}Pu and low enriched ^{235}U in saturated heterogenous Culebra dolomite. [10, Fig. 26] 30

Information Only

30. Heterogeneous fracture system in volcanic tuff with 10% matrix porosity and $^{239}PuO_2$ deposition in 0.5% fracture porosity with 20-cm fracture spacing (10.45% total porosity); water content in matrix set at 100%, 50% and dry; water content in fracture/fissile material set at 100% and dry.....30
31. Heterogeneous fracture system in Culebra dolomite with 10% matrix/vug porosity, and $^{239}PuO_2$ deposition in 0.5% fracture porosity with 20-cm fracture spacing (10.45% total porosity); Culebra brine content in matrix set at 100%, 50% and dry; brine content in fracture/fissile material set at 100% and dry. 32
32. Heterogeneous fracture system in 17% matrix/vug porosity with ^{239}Pu deposition in 1% and 4% fracture porosity and 20 cm fracture spacing. 32
33. Critical limits for 100% enriched ^{239}Pu and $^{239}PuO_2$ deposited as sphere in various homogeneous material at 20% total porosity saturated with water. [10, Fig. 27].....33
34. Criticality limits for 5% and 93% enriched U and UO_2 deposited as sphere in various homogeneous material at 20% total porosity with water and Culebra brine. 33
35. WIPP Salado brine substantially increases most critical limits for ^{239}Pu and $^{239}PuO_2$ deposited as sphere in various homogenous materials with 20% total porosity. [10, Fig. 28].....33
36. Salado brine increases critical limits for U and UO_2 at 5% enrichment deposited as sphere in various homogeneous materials with 20% porosity. 34
37. Critical radius for PuO_2 in various media with 20% porosity filled with water and WIPP brines.....34
38. Critical radius for UO_2 in various media with 20% porosity filled with water and WIPP brines 34
39. Critical mass usually decreases with increase in material porosity because influence of homogeneous media on reactivity decreases.[10, Fig. 29].....34
40. Concentration asymptote increases with porosity for media with small thermal neutron absorbing cross-sections, such as Culebra dolomite, and decreases with porosity for media with large thermal cross-sections, such as halite and rust.[10, Fig. 30].....35
41. Critical mass of 100% enriched ^{239}Pu and 93% enriched ^{235}U for homogeneous models in Culebra dolomite less than for heterogeneous models for both Culebra and Castile brines.....36
42. Critical concentration asymptote of 100% enriched ^{239}Pu and 93% enriched ^{235}U influenced by matrix porosity, pore fluid type, and fracture spacing in Culebra dolomite.....36

Information Only

TABLES

I. Projected uranium and plutonium mass for 1996, 2019, 2026 certifications, and 2023 Replacement Panels Planned Change Request at WIPP.[16, Table IV] 10
II. Minerals in Salado Halite and Culebra Dolomite. 11
III. Weight percentages of element oxides of minerals associated with WIPP disposal system. 12
IV. Total porosity of Culebra dolomite for various fracture, vug, and matrix porosities. 12
V. Composition of Culebra, Salado, and Castile brines near WIPP. 13
VI. Projected mass of components of TRU waste in CRA-2019 and CRA-26-19P. [16, Table II, 22, Tables 5-5, 5-6, 5-7, 25] 20
VII. Comparison of plutonium mass in spherical core in tuff at 10% matrix porosity, 0.5% fracture porosity, 20 cm fracture spacing for current and literature analysis.[42, Table II] 31
VIII. Comparison of multiplication factor and reactivity in current with literature analysis for several static conditions of moisture in volcanic tuff fractures at 100% and 95.5% enrichment for ^{239}Pu and $^{239}PuO_2$. 31

Information Only

ACRONYMS AND INITIALISMS

ANS	American Nuclear Society
ANSI	American National Standards Institute
CCA	Compliance Certification Application (to EPA)
CH-TRU	contact-handled transuranic (waste)
CRA	Compliance Recertification Application (to EPA)
EIS	Environmental Impact Statement (for major federal projects required by *National Environmental Policy Act of 1969*)
EPA	US Environmental Protection Agency
LWA	WIPP Land Withdrawal Act
MCNP	Monte Carlo N-Particle transport code (for neutron and photon transport)
NRC	US Nuclear Regulatory Commission
PA	performance assessment
RH-TRU	remote-handled transuranic (waste)
RPPCR	replacement panel planned change request (to EPA)
SCALE	Standardized Computer Analysis for Licensing Evaluation (neutron and photon transport code)
TRU	transuranic (radioactive waste)
USL	upper subcriticality limit
WIPP	Waste Isolation Pilot Plant (repository in southeastern New Mexico for TRU waste from atomic energy defense activities)

Information Only

Information Only

I. INTRODUCTION

Like other nuclear facilities, the possibility of sufficient fissile mass and concentration causing a self-sustained neutron chain reaction (hereafter, succinctly referred to as criticality) must be evaluated for the Waste Isolation Pilot Plant (WIPP), an operating repository in southeastern New Mexico owned by the US Department of Energy for the geologic disposal of wastes containing transuranic (TRU) radioisotopes (Fig. 1).

In the past, concern about criticality occurring in a natural setting after closure of WIPP has been low because of the low mass of fissile material (mostly plutonium) dispersed throughout the containers (i.e., low initial concentration) and the tendency of fissile solute to disperse during transport, as discussed in 2001 and summarized in 2015.[1-3] However, waste destined for WIPP has expanded to include TRU waste in containers that allow larger combined mass limits in the transportation package.[4]

Hence, a renewed evaluation of the likelihood of assembling a critical mass after closure in or near WIPP has been undertaken for Compliance Re-certification Applications for 2019 and 2026 (CRA-2019[5] and CRA-2026, respectively). The renewed evaluation also supports (a) the replacement panel planned change request (RPPCR-23) to US Environmental Protection Agency (EPA),[6] and (b) a future supplemental environmental impact statement (EIS) for enlarging the WIPP repository to accept non-pit surplus plutonium material, when processed to meet WIPP waste acceptance criteria.[7, 8]

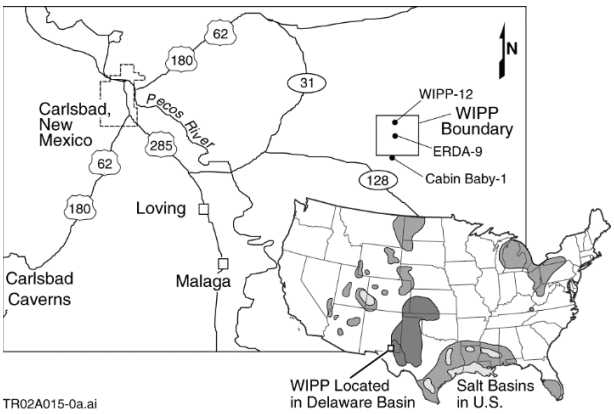


Fig. 1. WIPP repository 42 km east of Carlsbad in the Delaware Basin in southeastern New Mexico.[1, Fig. 1]

The post-closure criticality update for new waste streams is divided into four parts: (1) physical compaction of criticality control containers by disposal room closure through salt creep,[13, 14] (2) compaction of all other containers (such as pipe overpack containers and standard drums),[15, 16] (1) neutronic criteria necessary for post-closure criticality in geologic media,[9, 10] (3) hydrologic and geochemical constraints on fissile mass deposition,[11, 12] and (4) a summary of the low risk by combining the low probability and low consequences of criticality.[17] In support of the these reports, neutronic criteria necessary for post-closure criticality in geologic media have been calculated.[9, 10] This series of reports demonstrates that the possibility of post-closure criticality is remote and not necessary to include in WIPP performance assessments.

This article expands upon the neutronic conditions necessary for criticality to occur sometime in the future after repository closure; thus, the cause of deposition is not important to the discussion here. Study of criticality in a geologic setting is instructive because behavior of fissile material differs from common expectations. As a stand-alone article, this paper emphasizes this aspect of criticality.

This article updates previously published calculations for homogeneous spherical configurations in the repository and geologic barrier conducted for the 1996 Compliance Certification Application (1996 CCA) to EPA.[1, 3] Homogeneous mixtures, as discussed in §III, are often more reactive (i.e., neutron flux more effectively utilized) than heterogeneous mixtures, especially at high enrichments of plutonium and uranium.[18, Table III] However, the reactivity may increase in some configurations of lumped, heterogeneous mixtures of low enriched fissile material because the neutrons released in fission can migrate through the rock and brine and miss the large resonances in the non-fissile isotopes of fissile material. Consequently, the criticality potential of idealized heterogeneous mixtures, as discussed in §VII, is an addition to earlier analysis.

II WIPP DISPOSAL SYSTEM

II.A Fissile Mass in TRU Waste

EPA defined TRU waste that required deep geologic disposal as material contaminated with α-emitting TRU isotopes with an activity > 3.7 MBq/kg (>100 nCi/g) and half-life of >20 years.[19, 20] Two types of TRU waste allowed at WIPP, as defined in the *Waste Isolation Pilot Plant Land Withdrawal Act* (WIPP LWA),[21] are contact-handled transuranic (CH-TRU) waste and remotely handled transuranic (RH-TRU) waste from atomic energy defense activities. The volume of the projected inventory in each recertification has been less than allowed in WIPP LWA and so the inventory volume has been scaled to the legislated 175 564 m^3 waste volume allowed (Table I).

Information Only

Table I. Projected uranium and plutonium mass for 1996, 2019, 2026 certifications, and 2023 Replacement Panels Planned Change Request at WIPP.[16, Table IV]

	1996 CCA[14]		CRA-2019[22]				RPPCR-23-19P[23, 24]				CRA-26-19P[25]			
	1996		2033		12033		2083		12083		2083		12083	
Radioisotope	**CH (kg)**	**RH (kg)**	**CH (kg)**	**RH (kg)**	**CH (kg)**	**RH (kg)**	**CH (kg)**	**RH (kg)**	**CH (kg)**	**RH (kg)**	**CH (kg)**	**RH (kg)**	**CH (kg)**	**RH (kg)**
Uranium														
^{233}U	860	16	11	1.8	12	1.8	41	14	41	13	37	13	37	12
^{234}U	75	6.9	77	1.6	13	2.8	106	3.1	175	4.2	118	3.2	203	4.5
^{235}U	5 900	2 100	2 110	856	5 555	875	1 171	918	9 773	933	807	945	17 320	963
^{238}U	120 000	31 000	116 640	9 313	116 640	9 313	342 520	9 833	342 520	9 833	321 230	10 400	321 230	10 400
Enrichment ^{233}U+^{235}U	4.9%	6.5%	1.8%	8.4%	4.5%	8.6%	0.35%	8.6%	2.8%	8.8%	0.26%	8.4%	5.1%	8.5%
Plutonium														
^{238}Pu	15	0.09	55	1.3			74	1.2			92	1.4		
^{239}Pu	13 000	170	14 028	68	10 513	52	35 000	62	26250	48	67 200	73	50 400	56
^{240}Pu	920	222	1 392	14	487	5	3 038	16	1056	5.6	4 860	20	1 690	7.0
^{241}Pu	2.2	0.13	18	0.44			4.2	0.06			5.6	0.08		
^{242}Pu	310	0.04	38	4	37	5	62	4.9	61	6.3	73	6.1	72	7.7
^{239}Pu kg mass equivalent[a]	16 700	1 560[b]	15 500	622[b]	14 100	616[b]	35900	670	32600	660[b]	67 900	697[b]	61 600	771
Enrichment ^{239}Pu	91%	88%	90%	78%	96%	84%	92%	74%	96%	80%	92%	73%	97%	79%

[a] Pu fissile mass equivalent is the mass of ^{239}Pu plus factors for other fissionable masses: specifically, 0.113·^{238}Pu, 0.0225·^{240}Pu, 2.25·^{241}Pu, 0.0075·^{242}Pu, 0.9·^{233}U, 0.643·^{235}U, 0.015·^{237}Np, 0.0187·^{241}Am, 34.6·^{242m}Am, 0.0129·^{243}Am, 15·^{245}Cm, 0.5·^{247}Cm, 45·^{245}Cf, and 90·^{251}Cf. The factors derive from comparing the minimum critical mass of 0.45-kg ^{239}Pu (for a slurry, which includes bias and 0.02 margin on k_{eff}) to the minimum critical mass of other fissile isotopes.[26,Table XVI, 27,§5.2]

[b] Pu fissile mass equivalent for RH-TRU waste primarily derives from 0.643 ^{235}U

Two PAs/sensitivity analysis were performed for both RPPCR-23 and CRA-2026: (1) PA for an interim repository layout consisting of 12 panels (RPPCR-23-12P and CRA-26-12P, and (2) PA for final repository layout consisting of 19 panels (RPPCR-23-19P and CRA-26-19P). The 12-panel repository of RPPCR-23-12P, based on CRA-2019,[28] was approved by EPA in 2025.[29] However, 19 panels are necessary to accommodate the full SPD inventory; hence, we emphasize the 19 panel PAs herein: RPPCR-23-19P and CRA-26-19P.

The scaled ^{239}Pu enrichment in CH-TRU is 90%, 92%, 92% for CRA-2019, RPPCR-23-19P, and CRA-26-19P, respectively, and like the 91% projected in 1996 CCA (Table I). The scaled ^{239}Pu enrichment in RH-TRU is 78%, 74%, and 73% for CRA-2019. RPPCR-23-19P, and CRA-26-19P and <88% projected in 1996 CCA.

Because the other isotopes mixed with ^{239}Pu (such as ^{241}Pu and ^{235}U) influence criticality, the concept of fissile mass equivalent is used at WIPP to convert other fissile radionuclides in the TRU waste to an equivalent mass of ^{239}Pu (Table I). This approach for the fissile content bounds isotopic influences including changes with the decay over the 10^4-y regulatory period. Hence, for post-closure criticality evaluation, the fissile content is usually modeled as 100% ^{239}Pu. The assumed 100% enrichment increases reactivity but not excessively so (e.g., refer to Fig. 6 and Table VIII).

Although included in ^{239}Pu fissile mass equivalent concept, uranium is also considered separately from plutonium. The emplaced uranium enrichment at WIPP closure has remained less than the 4.9% projected in 1996 CCA. Specifically, the projected ^{235}U enrichment of CH-TRU at emplacement for CRA-2019 is 1.8% and for CRA-26-19P is 0.26%. However, the CH-TRU enrichment increases to 4.5% and 5.1%, for CRA-2019 and CRA-26-19P, respectively, over the next 10^4 years from the decay of ^{239}Pu (i.e., ~25% decay over 10^4 years with Pu half-life—$t^{1/2}_{^{239}Pu}$—of 2.406 × 10^4 y). The projected RH-TRU ^{235}U enrichment of 8.4% for both CRA-2019 and CRA-26-19P at WIPP closure is somewhat larger than the 6.5% enrichment projected in 1996 CCA (Table I). The enrichment of RH-TRU remains fairly constant over the next 10^4 years (the ^{235}U enrichment only increases to 8.6% and 8.5%, respectively).

Based on the large CH-TRU inventory and small RH-TRU inventory, the uranium enrichment is mostly modeled as 5%, though enrichments up to 93% are also used when lower enrichments are not critical.

II.B. Geologic Characteristics of WIPP Disposal System

II.B.1. Salado Formation

The 600-m-thick Salado Formation hosts the WIPP repository 654 m below the surface. Near the repository, the Salado consists of nearly horizontal (<1° regional dip) rock salt and interbeds of anhydrites and thin clay.[1, Fig. 4] The rock salt is mostly halite with <5 wt. % mineral impurities. The impurities, either as intergranular coatings or discrete fine particles, are polyhalite,

Information Only

anhydrite, gypsum, magnesite, various clays, and quartz derived from the clay (Table II).[30] Because of the small amount of mineral impurities in the WIPP rock salt, calculations herein use 100% halite (NaCl).

Table II. Minerals in Salado Halite and Culebra Dolomite.

Mineral (i)	Density (ρ_i) (kg/m^3)	wt %	vol %[a]
Salado Salt			
Halite, NaCl	2163[34, 35]	93.23[b]	94.52
Polyhalite, $K_2Ca_2Mg(SO_4)_4 \cdot 2H_2O$	2775[36]	1.53	1.21
Anhydrite, $CaSO_4$	2963[35, 37]	1.53	1.20
Gypsum, $CaSO_4 \cdot 2H_2O$	2320	1.53	1.45
Magnesite, $MgCO_3$	3009	1.53	1.12
Clay Corrensite	2800	0.64[b]	0.50
Average grain density	2195		
Culebra Dolomite[38, p. 3-9]			
Dolomite, $CaMg(CO_3)_2$	2840	91.5	90.71
Clay			
Corrensite $(Ca_{0.6}\ Na_{0.2}\ K_{0.2})(Mg_5\ Fe_3\ Al)(Si_6\ Al_2)O_{20}\ (OH)_{10} \cdot 9H_2O$	2800	2.4	2.41
Illite $(K_{0.6}(H_3O)_{0.4})\ (Al_{1.3}\ Mg_{0.3}\ Fe_{0.1})\ S_{3.5}\ O_{10}\ (OH)_2 \cdot H_2O$	2750	1.6	1.64
Gypsum, $CaSO_4 \cdot 2H_2O$	2320	3.0	3.64
Quartz, SiO_2	2650	1.5	1.59
Average grain density	2816		

[a] $vol\%(i) = \dfrac{wt\%(i) / \rho_i}{\sum_j wt\%(j) / p_j}$

[b] Halite wt % was measured; silcate residue wt % was measured and assumed to be corrensite clay; other minerals were set at equal values for the remaining wt %[39, p. 81]

II.B.2. Culebra Dolomite Member of Rustler Formation

The Rustler Formation overlies the Salado. The 7.3-m thick Culebra Dolomite Member of the Rustler Formation, 216 m below the surface, is the most likely pathway for transporting radionuclides away from the repository after an inadvertent human intrusion because it is the most permeable saturated strata relative to other stratigraphic units above the WIPP repository.[31, 32]

The Culebra is divided into four units near the WIPP repository (Fig. 2).[2, Fig. 5 33] The uppermost unit, Culebra Unit 1, averages 2.99 m in thickness but is not transmissive with only a small number of large-scale discontinuous fractures that occur along bedding planes, and some microvugs. Originally, vugs were anhydrite pockets that hydrated to gypsum during sedimentation; subsequent dissolution of gypsum left the vugs.

The middle Culebra Units, 2 and 3, are similar with small-scale fracturing. Culebra Unit 2 is about 1.60 m thick; Culebra Unit 3 is about 1.20 m thick (Fig. 2). Because of more extensive fracturing, intact pieces of core from Culebra Unit 3 are rare. The fractures in both units are either open or gypsum-filled, with apertures up to 2 mm wide. Micro fractures (< 0.05 m long and spaced 1 to 10 cm) and randomly oriented fractures (0.05 m to 0.2 m long and spaced 2 to 20 cm) are abundant. Sub vertical fractures (0.2 to 1 m long and spaced <50 cm apart) and bedding plane fractures (< 1 m long and spaced 5 cm to 40 cm) are common. The longer fractures connect abundant microvugs (< 3 mm in diameter) and some large vugs (0.3 cm to 10 cm in diameter).

The lowermost Culebra Unit 4 is typically 1.55 m thick near the repository (Fig. 2). Small-scale undulatory bedding plane fractures, sub vertical fractures (spaced 5 to 50 cm), and randomly oriented fractures are common. Microvugs are present at the top of Unit 4. Occasionally, large vugs (< 8 cm in diameter) occur near the bottom of Unit 4 but are not well connected by fractures.

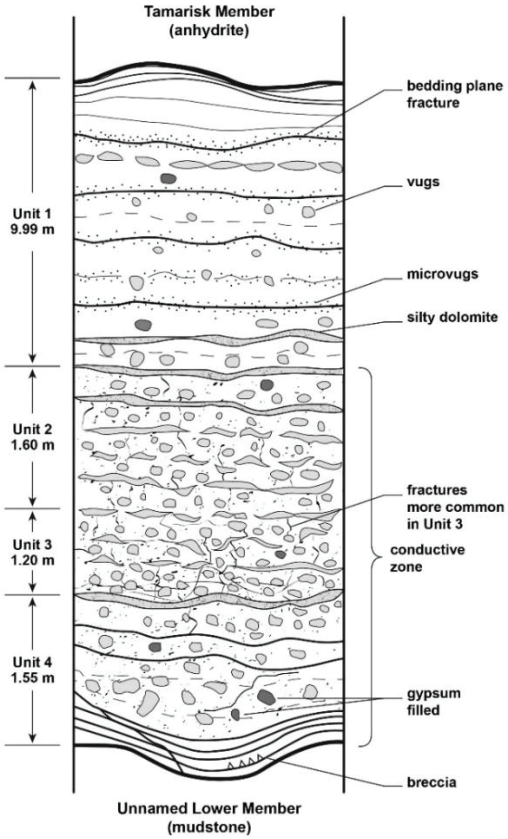


Fig. 2. Stratigraphic divisions of Culebra Dolomite Member of Rustler Formation.[40, Figure 3-6]

The Culebra consists mostly of dolomite (85% to 90%) followed by clay (3% to 5%), gypsum, and quartz (Table II).[38, p. 3-9] In WIPP-12 well (Fig. 1), the clay consisted of corrensite (60%), illite (33%), and minor

Information Only

amounts of serpentine (3%), and chlorite (4.5%).[38, Table 3-1] For criticality calculations, clay was assumed to comprise 4% of the mass with 60% corrensite and 40% illite (Table II).

The Culebra dolomite consists primarily of Ca and Mg elements. No other materials around WIPP contain a high percentage of Ca and Mg, except for the cement mixture, which is a hypothetical mixture that mimics behavior of the adulterant added to reduce attractiveness of disposed surplus Pu (Table III).[41, Table IV-4]

Table III. Weight percentages of element oxides of minerals associated with WIPP disposal system.

Element Oxides	Culebra Dolomite[a] (wt %)	Mont-morillinite[b] (wt %)	NRC Concrete[c] (wt %)	Cement Mixture[c] (wt %)	Oklo Sandstone[d] (wt %)	Yucca Tuff[e] (wt %)
SiO_2	1.55	43.77	72.09	58.50	84.10	77.00
CaO	29.39	1.02	6.16		0.02	0.53
MgO	21.08			19.80	0.68	0.16
Al_2O_3	0.26	18.57	6.42	11.70	7.70	12.70
Fe_2O_3	0.22[f]		2.00		2.50	0.85[ef]
K_2O	0.09				1.84	4.97
Na_2O	0.10	1.13	3.91		0.06	3.64
TiO_2					0.19	0.10
Mn_3O_4					0.02	0.06[g]
SO_3	3.30					
P_2O_5						0.01
H_2O		36.09	8.94	10.00		
CO_2 (ignition loss)	44.03				1.97	
Total	100.00	100.58	99.51	100.00	99.08	100.00
Density (ρ^{grain})	2820	2350	2300	2400	2660	2200

[a] Ref[41, Table IV-4]; WIPP-12 at 246.7 m depth (Fig. 1)
[b] webmineral.com accessed 12-5-18; based on *Eur. J. Min.* **9**:821-827 (1997); composition based on empirical formula
[c] Ref[42, Fig. A-3], including 10% water
[d] Ref[43, Table 3]; near natural reactors where not much silica dissolved and where <0.10% UO_2
[e] Ref[44, Table I]; similar to Ref[45] and composition average of Tptpmn, Tptpll, and Tptpln stratigraphic modeling units at Yucca Mountain[46, App. A]
[f] Reported as FeO
[g] Reported as MnO

The total (or bulk) porosity of the Culebra Dolomite Member of the Rustler Formation is a combination of vug ($\phi_{Culebra}^{vugs}$), fracture ($\phi_{Culebra}^{frac}$), and matrix porosities ($\phi_{Culebra}^{matrix}$)(Table IV):

$$\phi_{Culebra}^{total} = \phi_{Culebra}^{frac} + (\phi_{Culebra}^{matrix} + \phi_{Culebra}^{vugs})(1 - \phi_{Culebra}^{frac}) \quad (1)$$

The unconnected micro-vug porosity $\phi_{Culebra}^{vugs}$ of the lower 3 units is ~ 5%. Based on measurements of intact well core, the diffusive porosity ($\phi_{Culebra}^{matrix} + \phi^{vugs}$ and expressed as $\phi_{Culebra}^{matrix+vugs}$ hereafter) has been set between 10% and 25% with a median and mean of 16% since 1996 CCA.[33, 47, App. PAR, 48, Fig. 2.-10 & Table 2.6-3]

Based on tracer tests in 1996, the advective fracture porosity ($\phi_{Culebra}^{frac}$) of the lower 3 units is log-uniformly distributed between 0.01% and 1% with 0.1% median and 0.2% mean in WIPP performance assessments (PAs).[49, Fig. 23] An advective fracture porosity of 4% was also used in early PAs and is sometimes used here as a bounding value. The advective fracture porosity includes connection to some vug porosity. As apparent from Table IV, the total porosity is primarily from the matrix porosity at the median advective porosity of 0.1% (or mean advective porosity of 0.2% but not shown).

Table IV. Total porosity of Culebra dolomite for various fracture, vug, and matrix porosities.

Advective $\phi_{Culebra}^{frac}$ (%)	Diffusive $\phi_{Culebra}^{matrix+vugs}$ (%)	Total $\phi_{Culebra}^{total}$ (%)
4.0	10	14
	15	18
	17	20
	20	23
	25	28
1.0	10	11
	15	16
	17	18
	20	21
	25	26
0.1	10	10
	15	15
	17	17
	20	20
	25	25

Information Only

In WIPP PAs, the connected fracture spacing is uniformly distributed between 10 and 100 cm with mean/median of 55 cm, based on tracer well tests.[47, App. PAR, 49] For academic interest, smaller values between 1 to 20 cm, which correspond to the unconnected micro fractures in Units 2 and 3, are also examined.

I.B.3. Brine Compositions for Calculations

Three brines are considered near the WIPP repository in the criticality calculations. The brine in the Culebra dolomite above the WIPP repository, as measured in the Air Intake Shaft, is only slightly more saline than brackish water (Table V).

The Salado rock salt contains a small amount of interstitial brine not bound in hydrous minerals or fluid inclusions (~0.3 wt. % in clear halite, ~1.5 wt. % in argillaceous salt, and ~2.2 wt. % in clay seams).[50] The Salado brine composition is based on weeps at the repository horizon (Table V).[51, 52]

Within the land-withdrawal boundary of WIPP (Fig. 1), a pressurized brine reservoir was intersected in the 500-m thick Castile Formation (which underlies the Salado Formation) by one exploratory borehole (WIPP-12) during site characterization.[47, Appendix DEL, Section 7.5, 53] Hence, WIPP PAs assume that Castile brine could enter the repository through a new exploratory borehole in the next 10^4 years. The Castile brine composition, based on an early exploratory borehole ERDA-6, has substantially less magnesium (Mg^{+2}), potassium (K^{+1}), chloride (Cl^{-1}), and boron (B^{+3}) than Salado brine (Table V).[39, 54, 55] The Cl^{-1} and B^{+3} are particularly important for post-closure criticality evaluation, but Mg^{+2} has some influence.

Both brines will react with the contents of disposal room such as iron and lead in the containers and thus, contain Fe^{+2} and Pb^{+2} in solution (Table V). In addition, magnesium oxide (MgO) is added to the rooms to combine with any carbon dioxide (CO_2) produced from degradation of organic material in the waste to keep the pH near neutral and buffer the solution. The final solution concentrations are dependent upon the minimum mixing volume anticipated in each WIPP certification for dissolving the Fe, Pb, and MgO inorganic elements and the organic ligands in the waste.[12, 52, 56]

Table V. Composition of Culebra, Salado, and Castile brines near WIPP.

Constituent	Brine Concentration (mM or mole/m³)					
	Culebra (Air Intake Shaft)	**Salado**[39] (1996) (Room Q)	**Salado**[52] (Current) (Weep Br[a])	**Salado**[52] (Reacted RPPCR[b])	**Castile**[52] (Reacted RPPCR[b])	**Castile**[53] (ERDA-6[c])
Sodium (Na^{+1})	600	4110	3530	4400	5100	4870
Magnesium (Mg^{+2})	21	630	1020	794	387	19
Potassium (K^{+1})	8.3	350	467	548	96	97
Calcium (Ca^{+2})	23	7.68	14	13	13	12
Boron ($B(OH_2)^{-1}$)	2.8	144	158	185	62	63
Lead (Pb^{+2})				11.4	5.37	
Iron (Fe^{+2})				0.0537	0.0569	
Chloride (Cl^{-1})	567	5100	5860	4970	5030	4800
Sulfate (SO_4^{-2})	77	303	177	210	174	170
Bromine (Br^{-1})	0.37	17.21	26.6	31.2	10.9	11
Bicarbonate (HCO_3^{-1})	1.1	12	16	0	0	16
Ionic strength	800	6700	6700	7920	7060	5300
pH	7.70	6.1	7.0	8.74	8.82	7.0
Total solids[d] (kg/m³)						
Calculated	43.37	335	365.1	358.2	332.8	310.0
Measured	42.6	355	368			313
Density (kg/m³)						
Calculated	1044.2	1223	1234.5	1230.1	1213.9	1199.3
Measured	1040.0	1230	1237.0			1201.0
Moderation Ratio	39.5	10.59	9.55	9.81	13.2	13.7

[a] Synthetic approximation of intergranular fluids of Salado Formation

[b] Based on brine in the disposal area, PA simulations interpolate between 5 brine volumes: minimum brine mixing volume and a factor of 2, 3, 4, and 5 times the minimum value. Values here assume a brine mixing volume of 33 800 m³, the minimum volume used in RPPCR-23-19P. CRA-26-19P uses a minimum brine mixing volume of 9608; thus, values here roughly correspond to a brine volume 3.5 times the minimum brine volume of CRA-26-19P.

[c] Synthetic approximation of early experimental well drilled to Castile Formation

[d] Brine refers to an aqueous solution with total dissolved solids (TDS) >50 kg/m³. Saline water 30 <TDS<50 kg/m³ with average sea water of ~35 kg/m³; brackish water has 5 < TDS ≤ 30 kg/m³; and fresh water has TDS ≤ 5 kg/m³

Information Only

We use the initial concentration in criticality calculations, because the minimum mixing volume may change in each WIPP certification and the influence on criticality is small. To elaborate, the composition of the reacted Castile is very similar to the original Castile brine (i.e., Cl^{-1} and Na^{+1} increase <5%) Except for the addition of Fe and Pb in solution and increase in dissolved Mg^{+2} (from 19 mM to 387 mM).[52, 56] As show in §III.C, this change does not influence Pu and U reactivity in Castile brine.

The composition of the reacted Salado brine changes more than occurs for reacted Castile brine (i.e., Cl^{-1} decreases 15%, Na^{+1} increase 25%, and B^{+3} increases 17%—Table V). Like the added MgO, Mg^{+2} in the Salado brine combines with the CO_2 such that its content decreases 22%. As shown below in §III.C, these larger chemical changes are still not enough to influence Pu and U reactivity in Salado brine.

III. CALCULATION OF CRITICAL CONCENTRATION AND MASS FOR HOMOGENEOUS SPHERE

A critical condition depends not only on the quantity of fissile material but also on its concentration, size, shape (which allow neutrons to leak out of the assembly), and any other material mixed with or surrounding the fissile material (which may absorb or reflect neutrons back into the fissile material).[18, p. 5] Setting limits for a heterogeneous mixture with specific shapes and masses of fissile and other material is complex. However, limits below which criticality is impossible can be calculated for homogeneous and heterogeneous mixtures of fissile material in a spherical shape, and these bounding limits are used here to provide guidance for more complex situations analyzed in companion reports.

III.A. Computational Tools

III.A.1 SCALE

As in 1996 CCA, we rely on neutron transport modeling tools to estimate quantities of fissile materials required in a geologic environment to achieve criticality. This approach is somewhat similar to the neutron transport modeling in geologic media that has been done to support development of well logging tools (e.g., [57]).

The minimum amount of fissile material necessary to create a critical assembly is a reflected sphere. For simple shapes of fissile material in geologic media, such as spheres, the most useful computational tool is the XSDRNPM module in the SCALE (Standardized Computer Analysis for Licensing Evaluation) system sponsored by Oak Ridge National Laboratory.[58] SCALE version 6.1 with the 238-neutron group cross-section set in the Evaluated Nuclear Data File/B version 7.1 (ENDF/B-V11.1) was used for the calculations reported here. The module XSDRNPM (which is a discrete ordinate, multi-group, deterministic code) has a particularly useful option to search for the radius of a sphere necessary to achieve criticality. XSDRNPM has been around for over four decades and has been extensively verified for this type of calculation.

Herein, a typical homogeneous calculation proceeds by first modeling an infinite sphere with a mixture of fissile and geologic material. This starting calculation also accounts for the temperature of the geologic material. Besides the number densities for the composition of the geologic material, fluid (brine or water), and fissile mineral, five parameters describe the homogeneous model (and are common to the heterogeneous model described in §VI): (1) volume void fraction of pores in geologic material (matrix porosity of the intact geomaterial in Table IV, $0<\phi_{mat}^{matrix}<1$), (2) void fraction occupied by fissile material ($0<f_{matrix}^{fissile}<1$), (3) fissile material enrichment, (4) depositional grain density of mineral form of fissile material ($\rho^{fissile}$), and (5) density of fluid filling pores (ρ^{fluid}), where

$$\rho_{mix}^{fissile} = \rho^{fissile}(\phi_{mat}^{matrix} f_{matrix}^{fissile}) \quad (2)$$

$$\rho_{mix}^{fluid} = \rho^{fluid}[\phi_{mat}^{matrix}(1-f_{matrix}^{fissile})] \quad (3)$$

$$\rho_{mix}^{rock} = \rho^{rock}(1-\phi_{mat}^{matrix}) \quad (4)$$

The characteristics of the nuclear cross-sections and self-shielding are evaluated with the BONAMI and CENTRM modules. Then, a series of calculations are made to find the minimum fissile concentration that causes an infinite sphere to go critical (i.e., a neutron multiplication factor of unity for an infinite sphere or k_∞=1).[a] These calculations establish the minimum asymptotic critical concentration for a finite sphere. The maximum concentration is the critical concentration of pure fissile material.

The next step sets up a SCALE model of a homogenous, finite spherical core of a mixture of fissile material and fluid in the pores of the geologic material.

[a]Generally, a fissile system is "critical" when a nuclear chain reaction is sustained, which is expressed by a neutron multiplication factor (k) of unity, where k is conceptually the number of neutrons in one generation divided by the number of neutrons in the preceding generation. Traditionally, k_{eff} denotes a multiplication factor for a system of finite extent, and k_∞ denotes a homogenous system of infinite extent.[59, pp. 75-84] As described in ANSI/ANS-8.1-2014,[27] k_{eff} is mathematically "the eigenvalue number that, when divided in the actual mean number of neutrons emitted per fission in an assembly of material, would make the calculated result for the nuclear chain reaction of that assembly critical."

Information Only

The core is surrounded by a spherical reflector of fluid and geologic material, free of fissile material, with 2 m thickness to represent a reflector of infinite extent.

A rough estimate of a critical radius for the finite spherical core is made, and the XSDRNPM module searches for the radius that causes criticality (i.e., an effective neutron multiplication factor of unity for a finite sphere or k_{eff}=1). Once the radius has been determined, the volume of the sphere and the critical concentration are used to calculate the minimum critical mass. The calculations step from the minimum asymptotic critical concentration to the maximum critical concentration to obtain the curve describing the relationship between fissile concentration and fissile mass.

III.A.2 MCNP

SCALE criticality limits are minimums found when linearly spacing out concentration, not the results of a systematic search to find the absolute minimum. Hence, a few models were also developed with MCNP (Monte Carlo code for solving Neutron and Photon transport equations) (Version 6.2) to find more a refined limit for a few geologic systems.[60] MCNP values are the result of a manual search for minimums starting with the SCALE values. MCNP values are used herein when available. In MCNP, the integral neutron and photon transport equations are solved with Monte Carlo techniques. The relative fractional error on the eigenvalue was 2.0×10^{-4} on all MCNP results.

III.B. Upper Subcriticality Limit and Bias

The limit for when a fissile configuration is considered critical is derived from the bias and uncertainties associated with the criticality code (SCALE or MCNP), the underlying nuclear data, and the modeling fidelity. In an engineered system on the surface with humans present, great care is taken to conservatively define the most appropriate upper subcritical limit (USL) to prevent criticality (i.e., USL = 1 – (code bias + bias uncertainty + administrative factor) where only unfavorable biases in comparison to benchmark experiments are considered).

Criticality experiments with common geologic materials have not been performed to validate results. Variation in porosity, saturation, and host rock composition in geologic systems have much more influence on the minimum masses and concentrations than calculational biases and uncertainties in k_{eff}. For example, USL varies by mineral form and is non-linear at low enrichments (e.g., for Rutherfordine—UO_2CO_3, the conservatism of a critical limit between 1.0 and 0.96 at 3% enriched is large compared to that at 93% enriched—Fig. 3).

As another example, uncertainty in the Salado brine composition has greater influence than calculational biases and uncertainties in k_{eff}. To elaborate, the Salado brine composition collected in weeps throughout the underground is used as the representative composition of Salado brine (with minimum mass of 2.97 kg and asymptotic concentration at k_∞ of 40.8 kg/m^3—Fig. 4a). Yet, a slightly different Salado brine composition was collected from the experimental Room Q and used in 1996 CCA (Table V).[39, 54, 55] Although the composition is similar, the reactivity[b] in Room-Q Salado brine is noticeably larger (minimum mass of 2.65 kg and asymptotic concentration of 37.4 kg/m^3—Fig. 4a)

Consequently, we assume USL is unity. Thus, a system is subcritical when $k_{eff} < 1.0$ throughout the article to be consistent between enrichments, brine composition, and mineral forms.[c] These criticality limits are used to demonstrate the low probability of criticality in radioactive disposal systems after closure when humans are absent, not for evaluating nuclear criticality safety during operations or transportation of fissile material when humans are present, based on consensus standards such as ANSI/ANS-8.1-2014.[27]

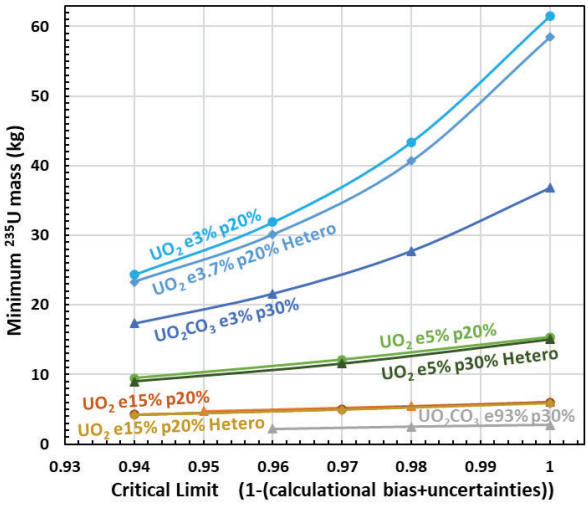


Fig. 3. Upper subcriticality limit for critical mass for ^{235}U as UO_2 and UO_2CO_3 in Culebra dolomite with 20% and 30% porosity saturated with Culebra brine is non-linear at low enrichment.[10, Fig. 4]

[b] Because of its use in §VII.D, we speak about the reactivity relative to Pu delayed neutrons (i.e., $\$ = (k_{eff} - 1) / 0.00212$), where 0.00212 is the fraction of delayed neutrons for Pu fission, rather than general $\rho^{crit} = (k_{eff} - 1) / k_{eff}$

[c] In recognition of the general uncertainty, critical limits in the following sections and figures are often reported to only 2 significant digits. An exception is §III.C, where we are comparing calculated critical limits to those reported in the literature.

Information Only

III.C. Critical Limits for Fissile-Fluid System

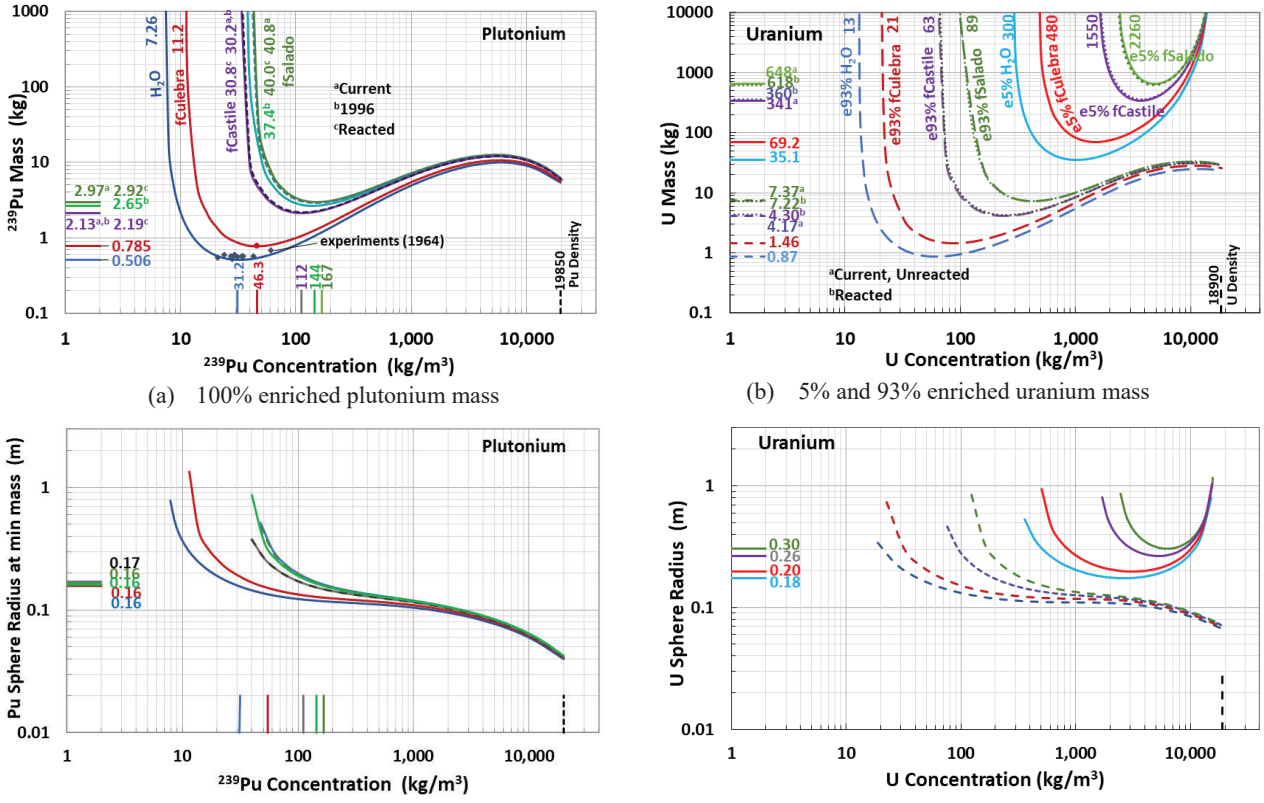
III.C.1 Plutonium-Fluid System

The minimum mass and minimum asymptotic concentration necessary in homogeneous fissile/fluid mixtures provide convenient bounds in the rationale for screening out the possibility of criticality after WIPP closure.

Based on calculations for ^{239}Pu in water mixture with k_{eff} of unity, the minimum ^{239}Pu mass is 0.506 kg at a concentration of 31.2 kg/m^3 in SCALE (versus 0.505 kg at a concentration of 31.9 kg/m3 in MCNP[10, Table VI]). The ^{239}Pu mass must exceed 0.506 kg for criticality to occur at any concentration of 100% enriched ^{239}Pu in pure water (Fig. 4).[d]

As the amount of water decreases, such that the ^{239}Pu concentration increases beyond 31.2 kg/m^3, the system becomes under moderated and the concentration of 100% enriched ^{239}Pu approaches the ^{239}Pu metal density of 19 850 kg/m^3 (as defined in SCALE) at a critical mass of 5.36 kg (i.e., k_{eff} at unity increases a factor of 10 from the minimum critical mass).

As the ^{239}Pu concentration decreases from 31.2 kg/m^3 through the addition of water, the system becomes over moderated. The necessary ^{239}Pu mass for criticality increases exponentially as the ^{239}Pu concentration asymptotically approaches 7.26 kg/m^3 where k_∞ is unity. Criticality is unlikely at ^{239}Pu concentrations less than 7.26 kg/m^3 (or for Pu fissile mass equivalent <7.26 kg/m^3 for mixtures with other fissile and fissionable radionuclides). However, placing the plutonium-fluid system in geologic media can lower the critical concentration, as discussed in §IV.



(a) 100% enriched plutonium mass

(b) 5% and 93% enriched uranium mass

(c) plutonium radius

(d) Uranium radius

Fig. 4. Calculated and measured critical mass and radius as function of fissile concentration in a homogeneous, spherical shape in water and WIPP brines:[1, Fig. 5, 10, Fig. 5, 61, Fig. 7, 62, Fig. 27-1, 63]

[d] When humans might be present, nuclear criticality safety limits for homogeneous Pu aqueous solutions are 0.48 kg, 7.3 kg/m^3, and 0.154 m cylinder/sphere diameter (provided concentration ^{240}Pu > ^{241}Pu and ^{241}Pu mass summed with ^{239}Pu).[27, Table I]

Information Only

The minimum critical Pu concentration asymptote is much larger in brine from the Castile and Salado Formations than water (Fig. 4a): a factor of 4.3 and 5.6 larger (30.2 kg/m^3 and 40.8 kg/m^3, respectively). The minimum mass is a factor of 4.2 and 5.9 larger than water (2.13 kg and 2.97 kg, respectively). Consequently, criticality is much less likely when Castile or Salado brine has entered the WIPP disposal region.

Furthermore, the concentration asymptote only increases 2.3% (30.8 kg/m^3) and the minimum mass only increases 2.8% (2.19) in reacted Castile brine. The concentration asymptote decreases only 2.0% (40.0 kg/m^3) and the minimum mass only decreases 1.7% (2.92 kg) in reacted Salado brine (Fig. 4a). Hence, we use the unreacted brine composition in calculations here.

At the minimum mass, most neutrons have been slowed into the thermal region through moderation. Hence, thermal absorption cross-sections (i.e., neutron absorption in the thermal region of the fluid or material) determines the minimum asymptotic concentration. Chlorine has a large thermal capture cross-section below 100 eV which depresses reactivity and so the critical concentration is larger than water.

The corresponding critical spherical radius at the critical concentration and mass is practically identical in water and dilute Culebra brine (0.16 m versus 0.15 m) and similar in Salado and Castile brines (0.18 m and 0.19 m). Although the necessary fissile spherical radius plateaus somewhat between 200 and 500 kg/m^3, the sphere radius continues to decrease monotonically to 0.04 m as the concentration increases to the ^{239}Pu metal density.

The calculated SCALE values for Pu/H_2O system are tightly spaced, thus, the refined MCNP values are similar. The Pu critical concentration asymptote is within 0.1% (7.22 kg/m^3 versus 7.23 kg/m^3). The Pu minimum critical mass is within 0.2% (0.506 kg versus 0.505 kg at a concentration of 31.2 kg/m^3 versus 31.9 kg/m^3). The corresponding radii are 0.157 and 0.156 m.

For the ^{239}Pu/H_2O mixture, the calculated criticality minimum mass compares well with compiled experiments and commonly cited values. An early 1964 compendium of experimental data reports ~0.510 kg (Fig. 4a) [62, Fig. 27-1]

In the 1981 analysis supporting ANSI/ANS 8.1-2014, normalized values of 0.522 kg, 0.513 kg, and 0.503 kg were calculated for PuO_2/H_2O solution and 0.532 kg, 0.525 kg, and 0.517 kg for $Pu(NO_3)_4$/H_2O solution using three different solution methods in the JOSHUA modeling system at Savannah River Laboratory. The reported results include bias adjustments but do not include an administrative factor of 0.02 on k_{eff}.[26, p. 80]

III.C.2. Uranium-Fluid System

The behavior for a 93% enriched ^{235}U system with water is similar to that of ^{239}Pu, and the critical mass and concentration asymptote increase substantially in WIPP brines (Fig. 4). For criticality to occur in a 93% enriched U/H_2O mixture, the ^{235}U solid concentration and mass must be respectively >12.3 kg/m^3 and >0.81 kg (Fig. 5a). The ratio of minimum ^{239}Pu mass to minimum ^{235}U mass is 0.625 (i.e., 0.506/0.81).

Like highly enriched Pu, a minimum radius does not occur for highly enriched U. For low enriched U, however, a minimum radius occurs that provides a geometric constraint for deposition (Fig. 4d).

The calculated criticality minimum mass for the 93% enriched ^{235}U/H_2O mixture, compares well with compiled experiments and commonly cited values. An early 1964 compendium of experimental data reports ~0.810 kg for 93.2% enriched ^{235}U (Fig. 5a),[62, 64, Table XXI] which is identical to 0.81 in Fig. 5a. In the 1982 analysis supporting ANSI/ANS 8.1-2014 for 100% enriched ^{235}U, values of 0.806 kg, 0.800 kg, and 0.805 kg were calculated for a UO_2F_2 aqueous solution using 3 different solution methods.[26, Table XXI]

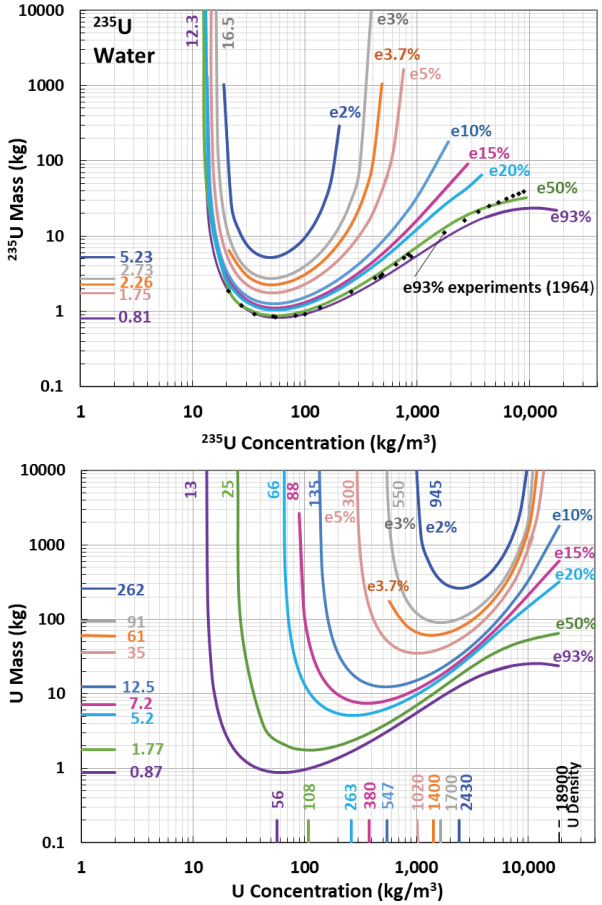


Fig. 5. Uranium calculated and measured critical concentration at various enrichments for a homogeneous, spherical shape in water.[10, Fig. 6, 61, Fig. 7, 62,

Information Only

[63] In WIPP Castile brine, the critical mass is 4.17 kg and in Salado brine, 7.37 kg for 93% enriched uranium. In reacted Castile and Salado brines, the mass increases 3.1% and decreases 2%, respectively.

For criticality to occur in a 5% enriched U/H_2O mixture, the U solid concentration and mass must be respectively >300 kg/m^3 asymptotic concentration and >35 kg (Fig. 5b). For 5% enriched uranium with too much water (i.e., over moderated with uranium concentration near 300 kg/m^3 at k_∞) the total mass of uranium must increase exponentially because neutrons are absorbed by the moderating water. With very little moderating fluid (i.e., under moderated with uranium concentration near uranium metal density of 18 900 kg/m^3—SCALE value), the uranium mass must increase substantially because enough water is not present to moderate neutrons sufficiently to be captured by ^{235}U.

In WIPP Castile brine, the minimum mass is 341 kg and in Salado brine 648 kg. The minimum mass increases 5.6% to 360 kg in reacted Castile brine and decreases 4.6% to 618 kg in reacted Salado brine (Fig. 4b). Thus, uncertainty in environmental conditions again has greater influence than computational uncertainties.

When expressed as ^{235}U rather than U, the minimum critical concentration range is quite narrow; the asymptotic concentration for 3% enriched uranium is 16.5 kg/m^3 and for 93% enriched, 12.3 kg/m^3 (Fig. 5b). Thus, the minimum critical concentration decreases as ^{235}U enrichment increases (Fig. 6). The minimum concentration also decreases as ^{239}Pu enrichment increases (Fig. 6).

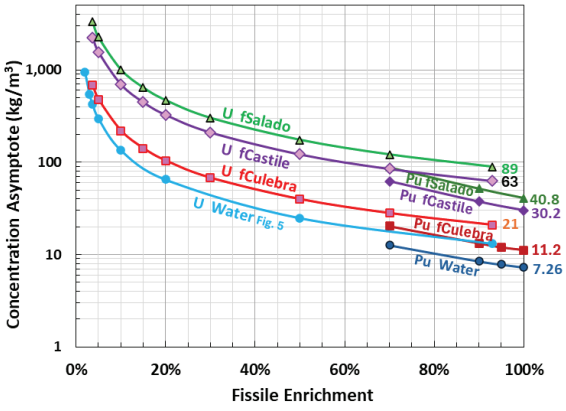


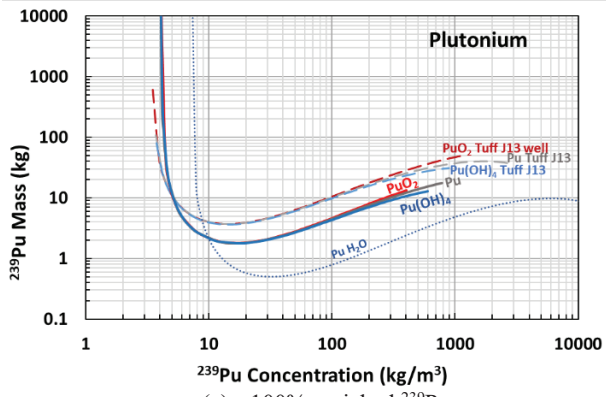
Fig. 6. Decrease of minimum critical concentration asymptote with increase in ^{239}Pu and ^{235}U enrichment in WIPP brines.[10, Fig. 7]

III.D. Minor Influence of Deposited Mineral Form at High Enrichment

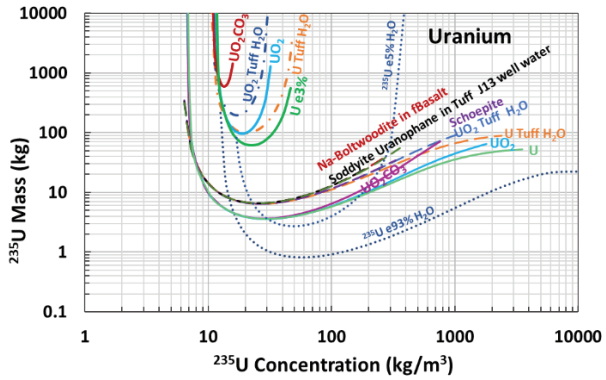
III.D.1. Mineral Forms of Plutonium

Plutonium is usually modelled as pure uncombined ^{239}Pu when it is mixed with fluids (such as brines in §III.C above), adsorbed on clay (as montmorillonite §IV.A below), or adsorbed on rust (as goethite §IV.B below).

Elsewhere, plutonium deposited in either the repository or the geologic barrier is usually modeled as plutonium dioxide (PuO_2 with ρ_g = 11 582 kg/m^3 and 88% of density as Pu^{IV}), rather than modeled with water of hydration or hydroxyl groups (i.e., $PuO_2(OH)_2{\cdot}H_2O$ or $Pu(OH)_4$). The mineral form influences criticality limits for highly enriched ^{239}Pu only when the mixture is under moderated (Fig. 7a).



(a) 100% enriched ^{239}Pu



(b) 3% and 93% enriched ^{235}U

Fig. 7. Pu and U mineral forms in Culebra dolomite/Culebra brine or volcanic tuff/fluid at 20% porosity.[10, Fig. 8]

The bound hydrogen in Pu minerals, such as $PuO_2(OH)_2{\cdot}H_2O$ or $Pu(OH)_4$), increases reactivity when under moderated (i.e., $Pu(OH)_4$, has lower critical mass than Pu or PuO_2 when under moderated in Fig. 7a). However, the influence of the bound hydrogen on

Information Only

reactivity is overwhelmed by aqueous water in most saturated configurations. [e]

Additional materials within or released from the TRU container, including neutron poisons and fission products, were neglected in the analysis here. Neglecting fission products and neutron poisons is very conservative but to determine how conservative would require significant effort to model the transport of all chemical species and is beyond the scope of this paper.

III.E.2. Mineral Forms of Uranium

Uranium is modeled as pure uncombined ^{235}U when uranium is mixed with fluids and adsorbed on clay or rust. Deposited uranium is modeled as uranium dioxide in the repository and the geologic barrier of the disposal system (UO_2 with ρ_g = 10 970 kg/m^3 and U^{IV} 88% of density). Uranium dioxide corresponds to the manufactured form of the fuel. Granted, uraninite is the depositional form that would occur in reducing regions of the disposal system, but the density change is minor (UO_2 with natural density between 10 600 and 10 970 kg/m^3).

Uranium deposition in the dolomite, above the WIPP repository, is also modeled as Rutherfordine (UO_2CO_3 with ρ_g = 5724 kg/m^3 and U^{VI} 72 wt. % of density) because it is the thermodynamically stable form for U^{VI} in a carbonate solution. Like Pu, depositional forms of highly enriched ^{235}U in Culebra dolomite have little influence on critical limits except when highly under moderated (Fig. 7b).

III.E. Influence of Deposited Uranium Minerals at Low Enrichment

In general, both the mineral form of the uranium and the material matrix (e.g., water, Culebra dolomite, or volcanic tuff) influences the critical mass at enrichments below 20% (Fig. 7 and Fig. 8). However, the mineral form only influences the critical mass when the uranium enrichment is <5% for two potential depositional minerals encountered in the Culebra dolomite of the WIPP disposal system, UO_2 or Rutherfordine—UO_2CO_3 (Fig. 8). Thus, the critical mass and asymptotic concentration limits for UO_2 are usually reported herein to simplify results.

Above 20% enrichment, the mineral form has no influence; only the material matrix influences the critical mass. Furthermore, the influence of enrichment is exponential above 20% enrichment (linear on log-log scale).

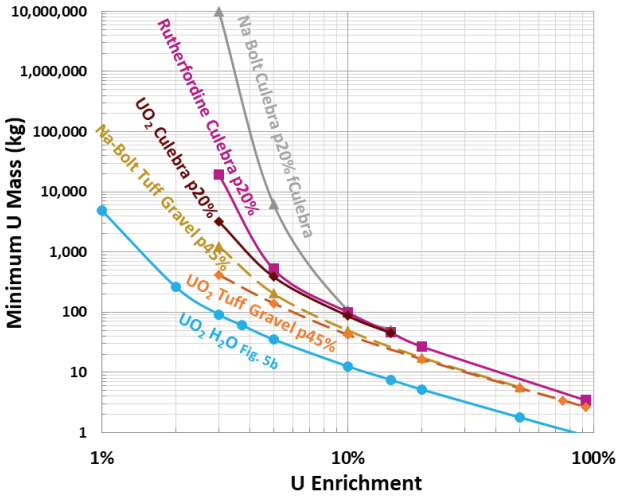


Fig. 8. Below 20% enrichment both Uranium mineral form and material matrix influences critical mass below 20% enrichment; only material matrix influences critical mass above 20% enrichment.[10, Fig. 9]

IV. CRITICAL LIMITS FOR HOMOGENEOUS SPHERE IN VARIOUS MATERIALS WITHIN REPOSITORY

The addition of geologic media to a fissile/water binary system usually substantially increases the mass of fissile material necessary to go critical for both ^{239}Pu and ^{235}U. However, well-hydrated material, such as clay, and carbon-rich material, such as graphite, are exceptions.

IV.A. Critical Limits in Carbon-Rich Material

IV.A.1. Cellulose

Between 5 790 t of cellulose (as estimated in CRA-2019) and 10 790 t (as estimated CRA-26-19P) may be disposed at WIPP, which is between 6% and 8% of the total CH-TRU material disposed (Table VI). Cellulose $(C_6H_{10}O_5)_n$ includes material with a wide variety of density such as cotton, woods (from balsa 125 kg/m^3 to 700 kg/m^3 hardwood oak), particle board, and fiber board (~400 kg/m^3). Most of the cellulose is inside the CH waste drums (Table VI), but here, the possibility of ^{239}Pu deposition in fiber board is modeled since fiber board is used as impact material in the pipe overpack container.[16] Cellulose acts as a weak moderator like sandstone discussed later in §V.B (Fig. 9).

[e] Similarly, the subcritical limits in ANSI/ANS-8.1-2014 apply regardless of the chemical form of the fissile nuclide. Specifically, [27,§5.2] "The subcritical mass limits for ^{233}U, ^{235}U, and ^{239}Pu in mixtures that might not be uniform [e.g., slurry that may have precipitated fissile material] are 0.50, 0.70, and 0.45 kg, respectively and independent of compound."

Information Only

Table VI. Projected mass of components of TRU waste in CRA-2019 and CRA-26-19P. [16, Table II, 22, Tables 5-5, 5-6, 5-7, 25]

Material	CRA-2019		CRA-26-19P	
	CH (t)	RH (t)	CH (t)	RH (t)
Fe-Based Metal	45 300	17 830	73 900	14 840
Cellulose	5 790	170	10 790	177
Plastics	9 700	882	12 680	1 400
Rubber	1 095	51	1 250	52
Cement	8 880	4	8 590	17
Total Material*	93 330	37 460	129 670	26 250

*Total material in repository including 5 listed materials

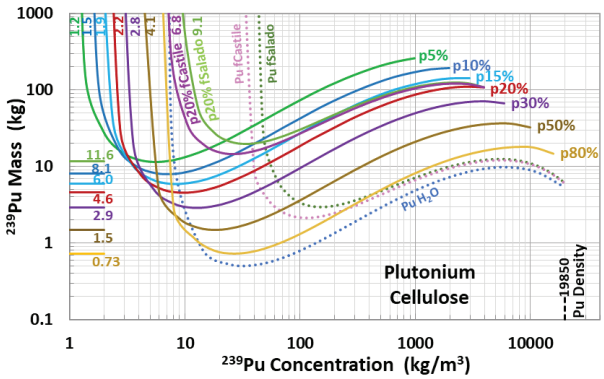


Fig. 9. Critical limits of plutonium mixed with water, WIPP brines, and cellulose at various porosities.

IV.A.2. Polyethylene

Polyethylene (CH_2—920 kg/m^3 density) is frequently used to bag Pu contaminated waste and is a component of the plastics category (between 9700 t and 12 680 t or between 10% and 8% of the total CH-TRU material disposed—Table VI). Here, we evaluate a spherical, homogenous mixture of ^{239}Pu polyethylene surrounded by polyethylene reflector. The critical mass is 0.36 kg (compared to 0.51 kg for water—Fig. 10). Polyethylene has slightly higher density of hydrogen and the carbon in polyethylene is a slightly better moderator than oxygen except at highly over moderated conditions.[65]

The 0.36 kg is identical to minimum mass first reported in 1977.[65] The critical mass drops to 0.26 kg for pure polyethylene with an upper subcritical limit (USL) set to 0.938 for transportation. The concentration asymptote is 8.5 kg/m^3 here but 9.0 kg/m^3 has been reported.[65]

Polyethylene bounds the behavior of hydrocarbons, and most other polymers (including condensation polymers, vinyl polymers, and acrylics) because the addition of other elements into hydrocarbons or polymers (such as oxygen, nitrogen, chlorine, fluorine, silicon, sulfur) decreases reactivity.[f] Only silicon grease polymer exceeds polyethylene but is not present in large amounts in TRU waste destined for WIPP.[66,p. 47]

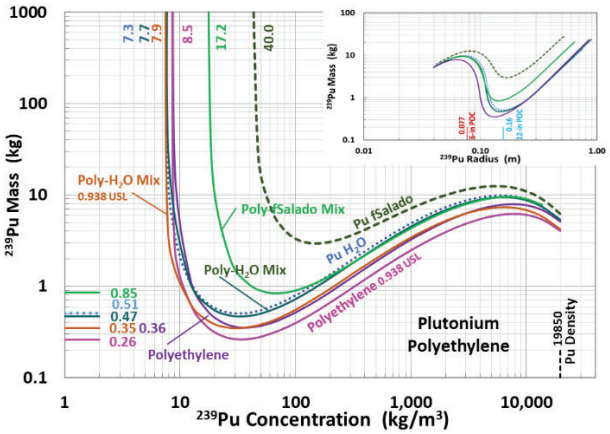


Fig. 10. Plutonium critical limits in polyethylene (100% and 74% volume), water (100% and 25%), Salado brine (100% and 25%), and beryllium (0 and 1%) with upper subcritical limit (USL) of unity and 0.938.

For a mixture of 74% volume of water, 25% polyethylene, and 1% Be, the minimum critical mass is 0.47 kg (versus 0.51 kg for 100% water). The minimum mass of a water/polyethylene mixture decreases to 0.35 kg for USL of 0.938, as used for transportation and discussed in a companion report.[16] For 74% Salado brine rather than water in the mixture, the minimum mass increases to 0.85 kg.

IV.A.3. Pure Carbon and Water

Although carbon is a large fraction of cellulose and polyethylene, pure carbon (or graphite) does not greatly increase the critical mass of Pu in water (e.g., 0.60 kg for carbon with 5% porosity or 0.64 kg with 20% porosity filled with water versus 0.51 kg in water—Fig. 11). However, carbon greatly decreases the critical asymptotic concentration for a fissile region of infinite extent because the carbon thermal absorption cross-section is smaller than water. For example, the critical asymptotic concentration in water is 7.2 kg/m^3 (Fig. 4)

[f] In February 2021, Oak Ridge National Laboratories, sponsor of SCALE, reported a small error (up to 1%) in the hydrogen kernel for polyethylene (but not for the hydrogen kernel for water) for SCALE versions 6.1.0 to 6.1.3 and 6.2.0 to 6.2.4. No differences were found in the minimum mass of 35.5214 kg when using the hydrogen kernel for water in polyethylene rather than the hydrogen kernel for polyethylene. Small differences occurred away from the minimum. For example, the asymptote for polyethylene was 8.575 kg/m^3 when using the water kernel and 8.533 kg/m^{3}when using the polyethylene kernel. The identical result at the minimum mass, and small differences (<0.5%) away from the minimum mass suggest that the small error in the hydrogen kernel for polyethylene is not important for the work reported here.

Information Only

while the critical asymptote in carbon is 0.48 kg/m^3 with 5% porosity filled with water (Fig. 11).

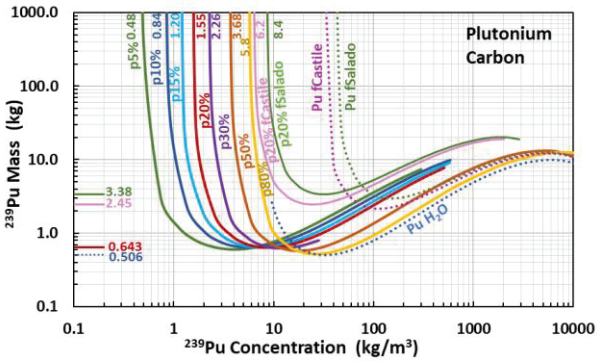


Fig. 11. Plutonium critical limits in carbon with porosity between 5% and 80% filled with water and WIPP brines.

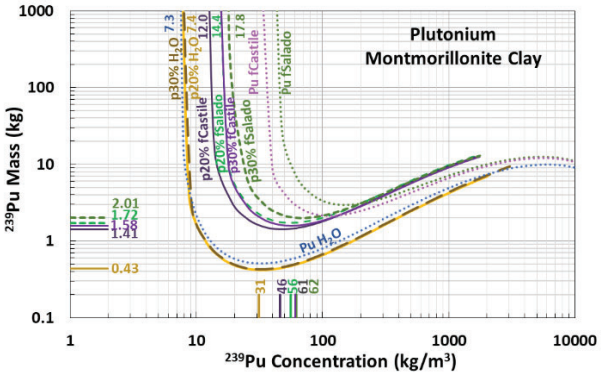
IV.B. Critical Limits in Hydrated Clay

Fissile material can adsorb on clays naturally present in fine layers of the Salado Formation and Culebra dolomite. In addition, bentonite clay, composed mostly of montmorillonite, is a likely engineered material to use in closing shafts and known boreholes within the WIPP disposal system (Table III).

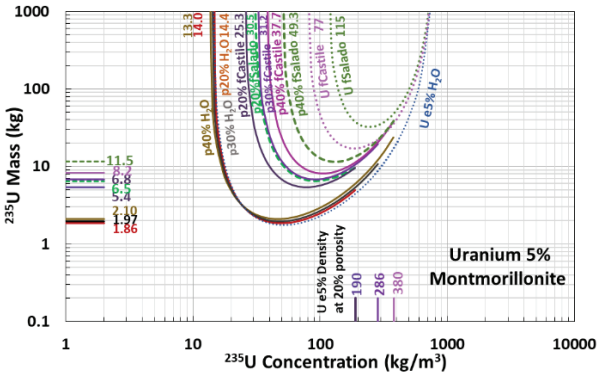
Montmorillonite is composed of three basic structural layers: a silicate sheet of silicon tetrahedron units (Si_4O_{10}) sandwiched between gibbsite sheets of aluminum octahedron units ($Al_2(OH)_6$), in which two out of every three OH^- ions are replaced with an oxygen of Si_4O_{10} (i.e., $Al_2(OH)_2$). For montmorillonite, some isomorphous substitution of Al^{+3} with Mg^{+2} has occurred within the gibbsite sheets.[67, p. 46] The charge imbalance from the substitution is compensated by the presence of an interlayer Na^{+1} and Ca^{+2} cations. Water molecules are readily absorbed in the interlayers between the montmorillonite structural groups. The clay greatly expands as water is absorbed by wetting and greatly contracts as water is removed by drying. When Ca^{+2} is the interlayer cation (most common), often two layers of water molecules are present; when Na^{+1} is the interlayer cation, between one and three water molecule layers are present.[68, p. 264]

Montmorillonite has the general chemical formula $(Na,Ca)_{0.3}(Al,Mg)_2Si_4O_{10}(OH)_2{\cdot}nH_2O$ with density between 2000 and 2700 kg/m^3. Here, we use a well hydrated composition of $Na_{0.2}Ca_{0.1}Al_2Si_4O_{10}OH_2{\cdot}10H_2O$ with density of 2350 kg/m^3 and molecular weight of 549.07 g/mol. Because of the high-water content in the clay (water of hydration is $10H_2O$), water in the porosity of the clay is immaterial for evaluating neutronic criteria (i.e., concentration asymptote of 7.17 kg/m^3 or 7.18 kg/m^3 and minimum mass of 0.443 kg or 0.445 kg at ~35 kg/m^3)

When the porosity is filled with either Castile or Salado brine, the behavior is not identical to a Castile or Salado binary system because of the pure water of hydration bound in the clay. Instead, the behavior straddles water and brine binary systems. The concentration asymptote for Montmorillonite clay is 12.0 kg/m^3 in Castile brine, and 14.4 kg/m^3 in Salado brine at 20% porosity. The critical mass is 1.41 kg in Castile brine and 1.72 kg in Salado brine (Fig. 12a).



(a) ^{239}Pu in montmorillonite clay[10, Fig. 10]



(b) 5% enriched U in montmorillonite clay

Fig. 12. Critical limits for montmorillonite clay with ^{239}Pu or ^{235}U (5% enriched) at 20% to 40% porosity saturated with water or WIPP brine.

Uranium behavior at 5% enrichment with clay is somewhat similar. When the fluid is water, the clay porosity has limited influence. The concentration asymptote varies between 14.4, 14.0, and 13.3 kg/m^3, for porosity of 20, 30, and 40%, respectively (Fig. 12b). The minimum mass varies between 1.86, 1.97, and 2.10 kg as ^{235}U. When the fluid is Castile brine, the behavior is between water and Castile brine because of the pure water of hydration in the clay. The concentration asymptote varies between 25.3, 31.2, and 37.7 kg/m^3. The minimum mass varies between 5.4, 6.8, and 8.2 kg as ^{235}U.

Information Only

IV.C. Critical Limits in Iron

Fissile material can adsorb onto corrosion products of the drums and metals in the waste within the repository, most notably iron corrosion products. Iron-based metals are between 49% and 57% of the total CH-TRU material disposed (Table VI). If the WIPP repository is somewhat oxidizing, the initial iron corrosion products of the steel may be particles of amorphous ferrihydrite (i.e., Fe^{+3}). Amorphous ferrihydrite (nominally am-$5Fe_2O_3 \cdot 9H_2O$ though the water content varies) may progress, through dehydration and aggregation, to more crystalline iron oxides, provided any absorbed metal cations do not block the transformation.[69]

Ferrihydrite is catalyzed (over months) by Fe^{2+} in brine to form iron hydroxychloride hibbingite ($Fe_2(OH)_3Cl$), magnetite ($Fe^{2+}Fe_2^{3+}O_4^{2-}$), goethite (α-$Fe^{3+}O(OH)$), lepidocrocite (γ-$Fe^{3+}O(OH)$—a polymorph of goethite with different crystal structure), or green rust (which is Fe^{2+} and Fe^{3+} cations in layered hydroxide anions (OH^-) with another anion such as Cl^-—$[Fe_3^{2+}Fe^{3+}(OH^-)_8]^+ \cdot [Cl^- \cdot nH_2O]^-$).[70, 71] Transformation of ferrihydrite to hematite (Fe_2O_3) can take longer.

We evaluate critical limits for homogeneous mixtures of goethite with Pu and U ions (Fig. 13), formed presumably through adsorption, because (a) formation of hematite can be lengthy, (b) magnetite does not contain hydrogen (which might reduce reactivity), (c) hibbingite contains Cl^- (which reduces reactivity and is already accounted for in the WIPP brine), and (d) formulas for ferrihydrite and green rust are indeterminate and may contain Cl^-. The porosity of iron oxides varies widely, and we use a porosity of 20% and 30% (Fig. 13).

In a mixture of Pu and goethite, the concentration asymptote and critical mass are greatly increased from that of Pu mixed solely with water because of neutron absorption by Fe (large thermal absorption cross-section). The concentration asymptote of a Pu/goethite/water mixture at 20% porosity is 18.6 kg/m^3 (0.61 wt. % dry) (versus 18.5 kg/m^3 in MCNP[10, Table VI] (Fig. 13).[1, Fig. 10]

Although the concentration asymptote and critical mass increases when the fluid is brine, the increase is small for either Castile or Salado brine. Furthermore, the goethite porosity does not have much influence (i.e., the critical concentration asymptote is 24.8 kg/m^3 (0.87 wt. %) in goethite at 20% porosity filled with Salado brine and 22.8 and 23.6 kg/m^3 in goethite at 20% and 30% porosity, respectively, filled with Castile brine—Fig. 13).

For 93% and 5% enriched UO_2, the concentration asymptote is 51.6 kg/m^3 and 1490 kg/m^3 (34 wt.%), respectively, as 20% porosity in Castile brine (Fig. 14).

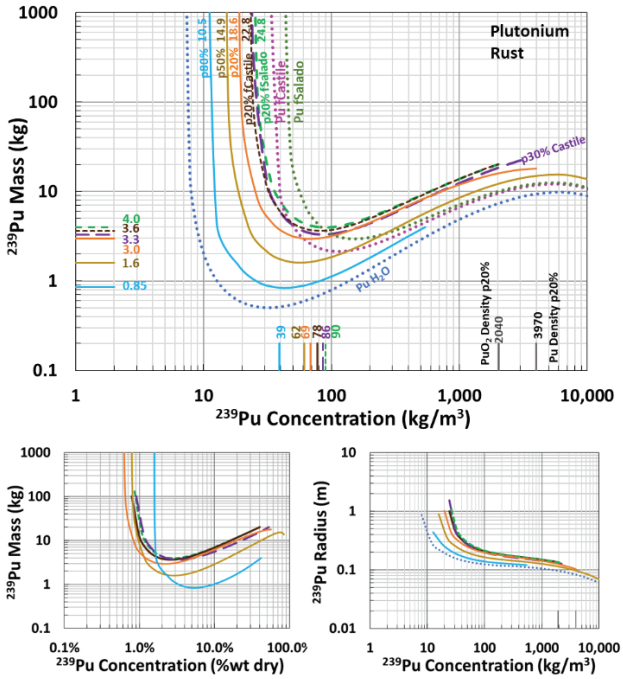


Fig. 13. Critical limits of Pu in goethite (Fe rust) at 20% and 30% porosity filled with water and WIPP brines.[10, Fig. 13]

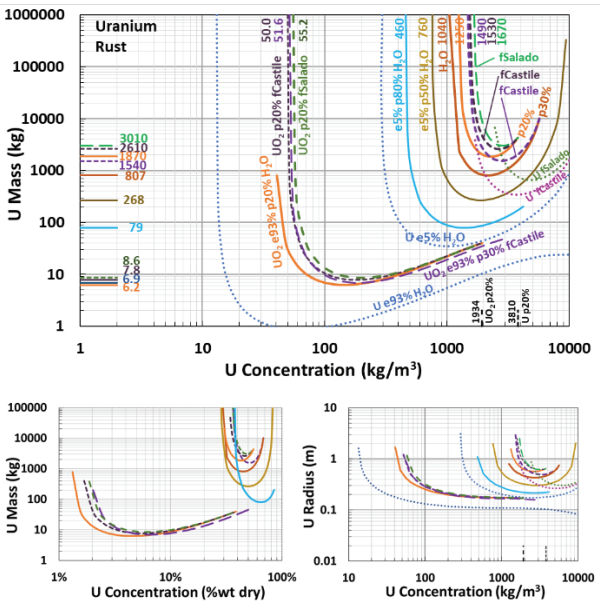


Fig. 14. Critical limits of 93% and 5% enriched uranium in goethite (Fe rust) at 20% and 30% porosity filled with water and WIPP brines. [10, Fig. 13]

Information Only

V. CRITICAL LIMITS IN SILICON-RICH MATERIALS

Silicon (SiO_2), acting as a weak moderator, reduces the concentration asymptote to less than for water. Silicon-rich materials considered here include concrete and sandstone. Other silicon-rich materials behave similarly, such as volcanic tuff at Yucca Mountain as discussed in §VII.B,[46, App. A].

V.A. Critical Limits in Cement/Concrete

Reacted and unreacted cement is ~10% of the projected total CH-TRU waste material to be disposed at WIPP in CRA-2019 and ~6% in CRA-26-19P (Table VI). Deposition of mobile Pu might also occur in concrete structural components of the WIPP repository (e.g., drifts, shafts, and boreholes). Cement in concrete does not have a fixed composition, but the major components are SiO_2, CaO, MgO, Al_2O_3, Na_2O, and Fe_2O_3. Here, a cement composition high in SiO_2 content was used as specified by the Nuclear Regulatory Commission (NRC) (Table III). The NRC-concrete is varied between 10% and 30% (Fig. 15).

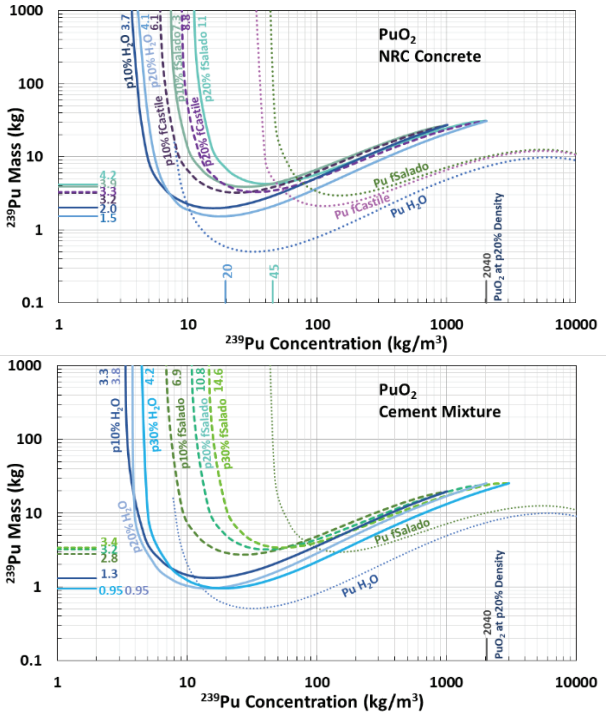


Fig. 15. Critical limits of PuO_2 in NRC concrete and cement mixture with porosities between 10% and 20% filled with water or WIPP brine. [10, Fig. 17]

In comparison to PuO_2/water solution, the critical mass increases and the asymptotic concentration decreases as the matrix porosity decreases for a PuO_2/NRC-concrete/water mixture (Fig. 15). The asymptotic concentrations are less than a Pu/water solution because of the small thermal neutron cross-section of SiO_2 in the NRC concrete.

Interestingly, only the asymptotic concentrations decrease as matrix porosity decreases for a PuO_2/NRC-concrete/WIPP brine mixture. The critical mass shows only a small increase (Fig. 15). Hydrogen in the water is more readily available.

Critical limits of PuO_2 in a cement mixture were also evaluated. The cement components (Table III) bound the behavior of the adulterant that is mixed with surplus Pu for disposal at WIPP.[42] For a PuO_2/cement-mixture/water solution, the minimum mass also increases above that of PuO_2/water solution but not as much as NRC concrete. For a PuO_2/cement-mixture/WIPP-brine solution, the asymptotic concentrations decrease as matrix porosity decreases but the critical mass show less change than for NRC-concrete.

For 5% enriched UO_2 in water with NRC concrete, the concentration asymptote varies over a narrow range between 8.4 and 9.6 kg/m^3 for porosities between 10% and 30% (Fig. 16). In WIPP brine, however, the concentration asymptote varies widely between 16 kg/m^3 and 36 kg/m^3. The 5% enriched UO_2 critical mass varies a factor of 2 with NRC-concrete porosity when water fills the porosity (between 6 kg and 12.6 kg) and a factor of 1.75 when Salado brine fills the porosity (between 24 kg and 42 kg).

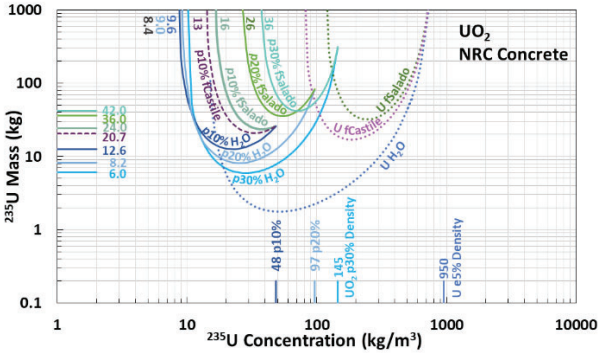


Fig. 16. Critical limits in NRC concrete for 5% enriched $^{235}UO_2$ at porosities between 10% and 30% filled with water or WIPP brines.

V.B. Critical Limits in Sandstone

Sandstone is not present near the WIPP facility, but uranium deposition, as UO_2, often occurs in permeable sandstone, which may be present in above or below other bedded salt deposits. In particular, a uranium ore body, which formed in a sandstone formation deposited 2.15 $\times 10^9$ years ago (2.15 Ga) in Gabon, Africa, had several locations that operated as natural reactors.[72] Most of the uranium in the Oklo ore body is of low grade (0.2 to 1 wt. % uranium).[43, Table 3, 73] However, some high concentrations of uraninite (UO_2) (>20 wt. % uranium with porosity between 20% and 40%) were formed, and

Information Only

within the high concentrations, some thin lenticular regions were critical 1.95 Ga when natural uranium had a content of ~3.7 wt. % ^{235}U (Fig. 17).

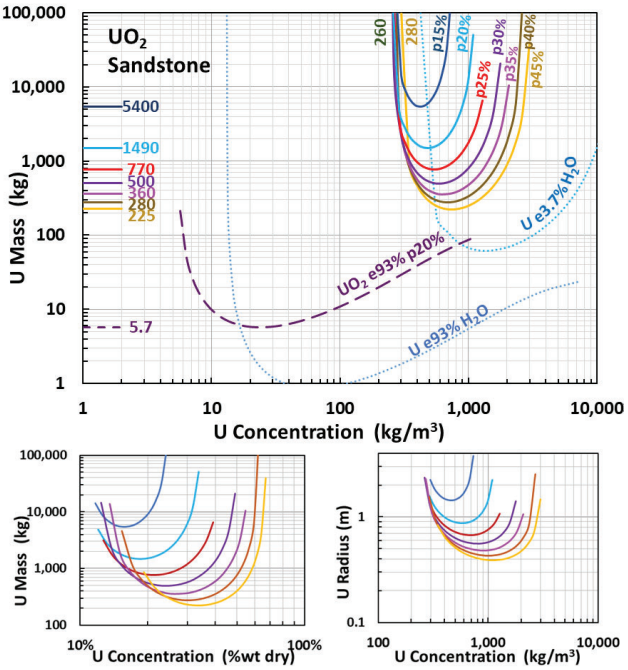


Fig. 17. Critical limits for 3.7% enriched UO_2 in sandstone at porosity from 15% to 45% filled with water.[10, Fig. 14]

For a homogeneous sphere of 3.7% enriched uranium in Oklo sandstone (Table III) to be critical requires deposition at a concentration found in high-grade ores (i.e., >240 kg/m^3 or 13 wt. % at 20% porosity).[g] The minimum critical mass varies between 1490 kg at 20% porosity, 500 at 30% porosity, and 280 kg at 40% porosity (Fig. 17).

For PuO_2 at 100% enrichment in homogeneous sandstone, the concentration asymptote is 3.3 kg/m^3 and the minimum critical mass is 2.85 kg at 20% total porosity (Fig. 18). These critical limits are somewhat similar to UO_2 at 93% enrichment: the concentration asymptote is ~5 kg/m^3 and minimum critical mass is 5.7 kg (Fig. 17).

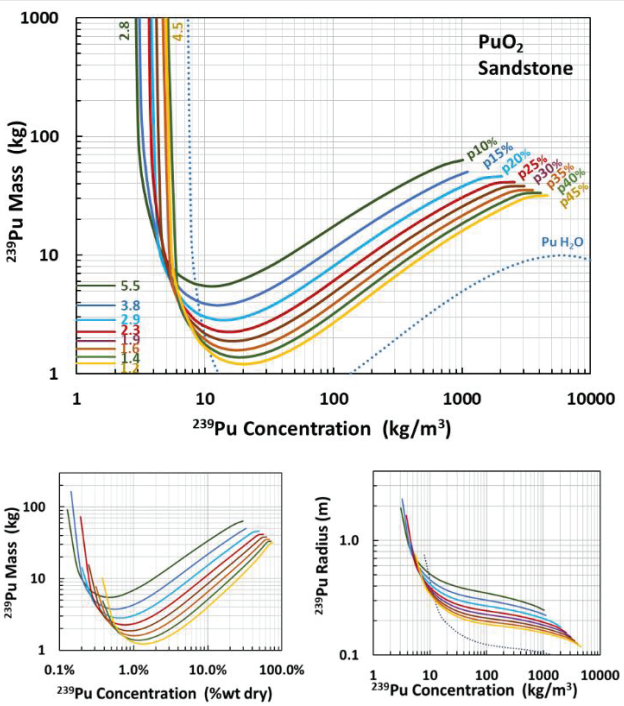


Fig. 18. Critical behavior for 100% enriched PuO_2 in sandstone at porosities between 10% and 45% filled with water.[10, Fig. 15]

VI. CRITICAL LIMITS IN EVAPORITES

VI.A. Critical Limits in Halite and Halite/MgO Mixture

PuO_2 migrating into the host halite or halite/MgO mixture surrounding containers filled with Salado brine is unlikely to form a critical assembly. As noted in §III.C, the asymptotic concentration of 40.8 kg/m^3 in Salado brine for PuO_2 is a factor of 5.6 larger than 7.26 kg/m^3 in water because of the neutron absorption by Cl^- [1] (Fig. 4a). The addition of a halite/MgO mixture or pure halite matrix increases the asymptotic critical concentration further. In halite/MgO mixture (in ratio of 1:1 by volume) at 10% porosity filled with PuO_2 and Salado brine, the asymptotic concentration reaches a maximum of 104 kg/m^3 (~3.9 wt. % in dry halite/mixture) (Fig. 19). In pure halite at 15% porosity, the asymptotic concentration reaches a maximum of 188 kg/m^3 (~9.3 wt. % in dry halite) (Fig. 19).[h]

In WIPP PAs, the intact salt porosity is fixed at 1% but could vary between 0.1% and 3%.[48] The excavation disturbed zone porosity is fixed at a central value of 5.5% but could vary between 1% and 10%.[48] For halite at 5%

[g]Researchers usually analyze Oklo reactors as thin cylinders to better match the thin lenticular shapes.[74] We use homogeneous spheres to be consistent with analysis reported here.

[h] Of all the materials examined herein, only salt and salt/MgO have a maximum asymptote between 0% and 100% porosity; for all other materials, the critical asymptote increases (or decreases) monotonically with porosity. The maximum is more readily apparent when plotting the asymptotes versus porosity (see §VIII.C).

Information Only

porosity, the critical concentration is 143 kg/m^3 (~6.4 wt. % in dry halite) (Fig. 19).

In a fissile/salt/brine mixture, the system is mostly under moderated because of the limited salt porosity. Because of the small matrix porosity available, the minimum critical mass occurs when fissile ^{239}Pu completely fills the halite/MgO or halite porosity (e.g., the minimum critical mass at 5% porosity occurs when the critical Pu concentration is at the density of PuO_2 with porosity 5%). Although not shown, the minimum critical mass in salt would decrease somewhat for pure Pu mineral because more ^{239}Pu can reside in the limited salt porosity for pure Pu with smaller volume than PuO_2.

The uranium disposed in CH-TRU at WIPP, which is <5.3% enriched in ^{235}U, will not go critical as $^{235}UO_2$ in halite or a halite/MgO mixture at a mass less than the total 18 283 kg present in CH-TRU and RH-TRU waste in WIPP after 10^4 years from decay of ^{239}Pu (Table I).[i]

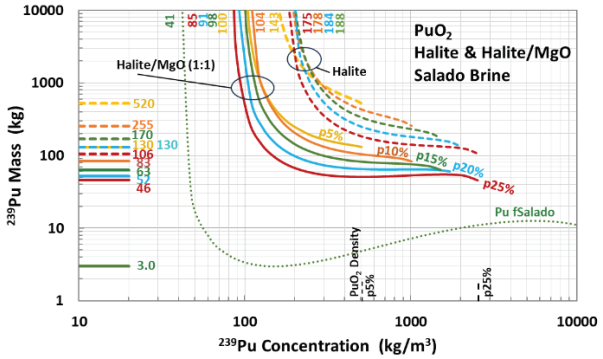


Fig. 19. Critical limits for PuO_2 in halite or halite/MgO matrix with porosity saturated with Salado brine.[10, Fig. 11]

VI.B. Critical Limits in Homogeneous Culebra Dolomite

For a homogeneous mixture of $^{239}PuO_2$ in Ca/Mg-rich Culebra dolomite saturated with Culebra brine at a total available porosity of 20%, the critical mass and asymptotic concentration are 2.1 kg and 3.7 kg/m^3, respectively (Fig. 20). To reach a critical concentration of 3.7 kg/m^3 in the Culebra dolomite, requires deposition conditions that would produce at least a low-grade ore (1300 ppm or 0.13 wt. % dry at 15% porosity in 2816 kg/m^3 dolomite with PuO_2 filling pores—Fig. 20).

A decrease in porosity in mildly moderating material shifts the curves to the left: for 18% total available porosity, the asymptotic concentration for criticality is 3.1 kg/m^3 and similar to the 3 kg/m^3 used in arguments screening out criticality for the 1996 CCA[1]. The critical minimum mass is 2.19 kg.

Culebra brine is fairly dilute and, thus, has critical limits similar to water (Fig. 4a); hence, the critical limits in Culebra dolomite saturated with water are similar: 1.6 kg and 3.1 kg/m^3, respectively (Fig. 21)

When the Culebra dolomite is saturated with Castile brine, as might occur when PuO_2 initially migrates into the Culebra after a borehole plug fails, the mass and asymptotic concentration are 4.2 kg and 8.5 kg/m^3, respectively, at 20% Culebra porosity (Fig. 21).

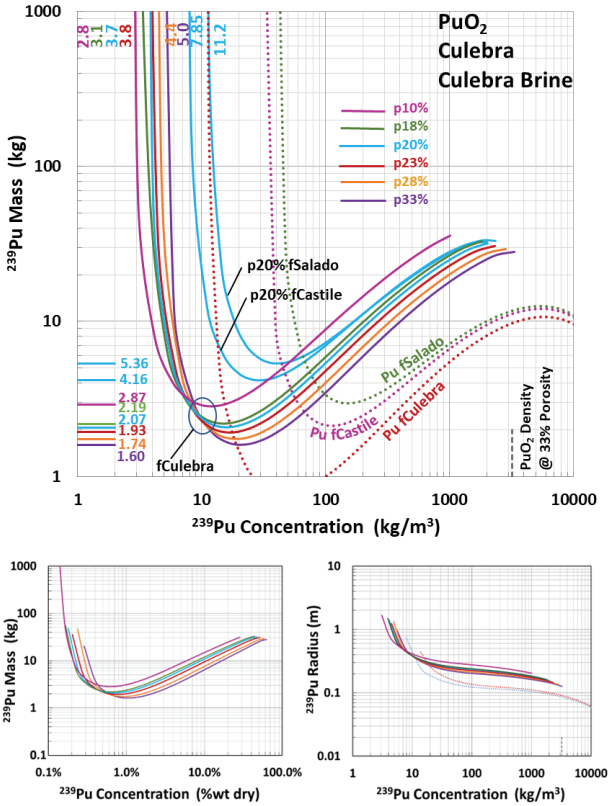


Fig. 20. Critical limits for PuO_2 in homogeneous Culebra dolomite with total porosity between 10% and 33% saturated with Culebra brine. [10, Fig. 18]

[i] An exact minimum mass was not calculated for 5% enrichment, since the numbers were so large. As an example, the $^{235}UO_2$ enrichment had to be increased to 15% in halite disturbed porosity of 10% before the minimum mass reduced to 2700 kg.

Information Only

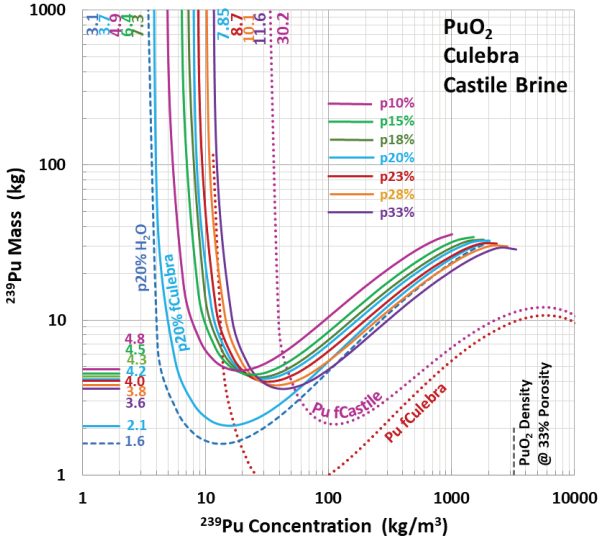


Fig. 21. Critical limits for PuO_2 in homogeneous Culebra dolomite with total porosity between 10 % and 33% saturated with Castile brine.

For uranium as uraninite ($^{235}UO_2$) 5% enriched, the concentration asymptote and critical mass are 9.95 kg/m^3 and 16 kg, respectively (Fig. 22a), for homogeneous Culebra dolomite where all 23% total porosity is available for deposition (i.e., 16% matrix, 5% vug, and 4% fracture porosity—Table IV). When expressed as U, the concentration asymptote and critical mass are 200 kg/m^3 and 320 kg, respectively, for 23% total porosity (Fig. 22a).

The maximum concentration when only the 4% fracture porosity is available for fissile deposition is 19.3 kg/m^3 as ^{235}U or 387 kg/m^3 as uranium (Fig. 22a). If only 1% fracture porosity is available for deposition (maximum fracture porosity typically modeled at WIPP—§II.B.2), then deposition of 5% enriched uranium is not critical.

As noted earlier in §III.E (Fig. 8), UO_2 (uraninite) and UO_2CO_3 (Rutherfordine) in a homogeneous mixture have similar critical limits for enrichment >5%, provided all the porosity is available for deposition. For example, UO_2 and UO_2CO_3 have the same critical concentration asymptote at an enrichment of 15% (54 kg/m^3—Fig. 23).

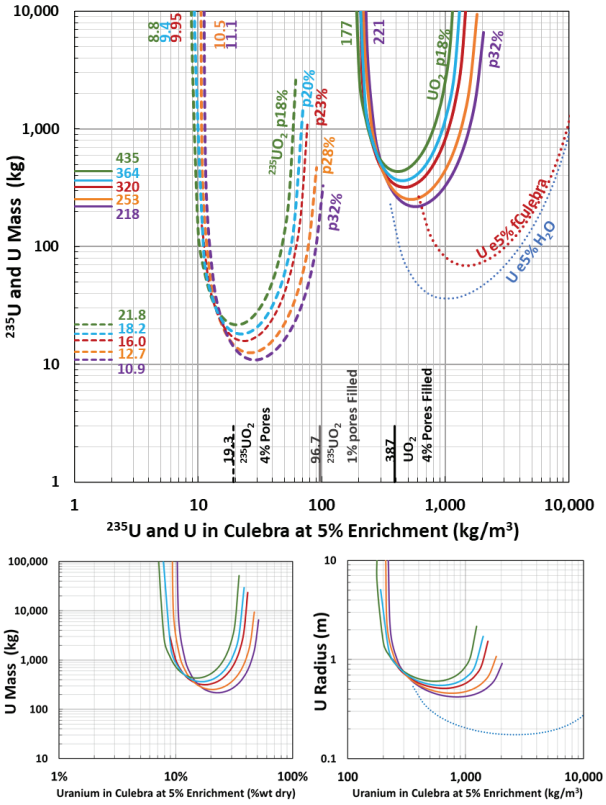


Fig. 22. Criticality limits for 5% enriched UO_2 in homogeneous Culebra dolomite with total porosity between 18% and 32% saturated with Culebra brine. [10, Fig. 19]

The minimum masses of UO_2 and UO_2CO_3 only differ slightly at 15% uranium enrichment (40 kg versus 42 kg, respectively—Fig. 23), because the 4% fracture porosity in the Culebra can accommodate the UO_2 mineral volume and most of the larger UO_2CO_3 mineral volume.

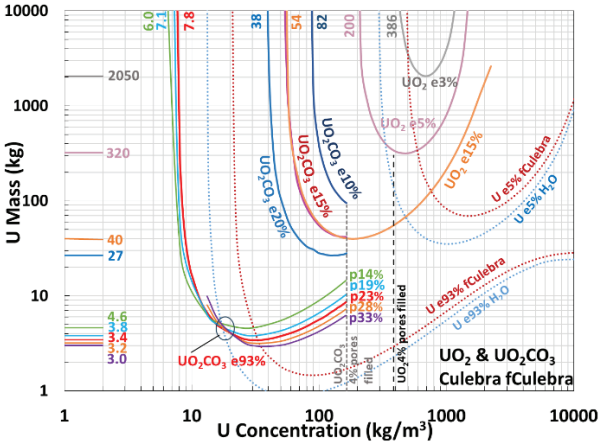


Fig. 23. Critical limits of uranium as UO_2CO_3 and UO_2 at various enrichments in homogenous Culebra dolomite mostly at 23% total porosity saturated with Culebra brine. [10, Fig. 20]

Information Only

However, the minimum critical mass differs for minerals of different sizes if the porosity is restricted. For example at 5% enriched uranium, a homogeneous model of the Culebra is critical at 320 kg when deposited as UO_2 with all the porosity available and critical at 333 kg if only 4% of the fracture porosity is available (Fig. 23), but is critical only at masses >>10^4 kg when deposited as UO_2CO_3 with only 4% fracture porosity available (not shown in Fig. 23).

VII. CRITICAL LIMITS CONSIDERING HETEROGENEITY IN CULEBRA DOLOMITE

VII.A. Approach for Fracture Heterogeneity

As noted in §II.B.3, the advective porosity of the Culebra dolomite is primarily along bedding planes and fractures. The matrix porosity may be inaccessible except by diffusion; thus, fissile deposition may only occur in the fracture porosity. To evaluate the heterogeneity effects, we developed a model of fissile deposition in fractures of the Culebra in SCALE. Modeling the heterogeneity of the rock-liquid-fissile material system with a Monte Carlo code such as MCNP or the KENO module in SCALE is difficult because of the large number of fractures potentially needed.

The conceptual model of the fractured Culebra dolomite consists of intact Culebra matrix with both matrix porosity and microvugs (Fig. 24). Parallel fractures with 2b aperture that are spaced 2B apart pierce the Culebra matrix. Brine can fill the dolomite matrix and fractures or only fill the fractures. The fractures may contain a mixture of fissile material and brine or just fissile material.

A computational unit cell is defined for the heterogeneous calculation with one fracture in the Culebra dolomite matrix. The pitch between the unit cells is the fracture spacing.

In addition to the 5 parameters for the homogeneous model, the heterogeneous fracture model requires 3 additional parameters for the fracture porosity: (6) fracture/void porosity (ϕ^{frac}), (7) fraction of the void that is filled with fissile material ($0< f^{fissile}_{frac} <1.0$), and (8) the fracture spacing (2B). Compared to homogeneous densities in Eq. (2) to Eq. (4), the mixture densities are

$$\rho^{fissile}_{mix} = \rho^{fissile}[\phi^{matrix+vug}_{Culebra} f^{fissile}_{matrix}(1-\phi^{frac}_{Culebra}) + \phi^{frac}_{Culebra} f^{fissile}_{frac}] \quad (5)$$

$$\rho^{fluid}_{mix} = \rho^{fluid}[\phi^{matrix+vug}_{Culebra}(1-f^{fissile}_{matrix})(1-\phi^{frac}_{Culebra}) + \phi^{frac}_{Culebra}(1-f^{fissile}_{frac})] \quad (6)$$

$$\rho^{rock}_{mix} = \rho^{rock}(1-\phi^{matrix+vug}_{Culebra})(1-\phi^{frac}_{Culebra}) \quad (7)$$

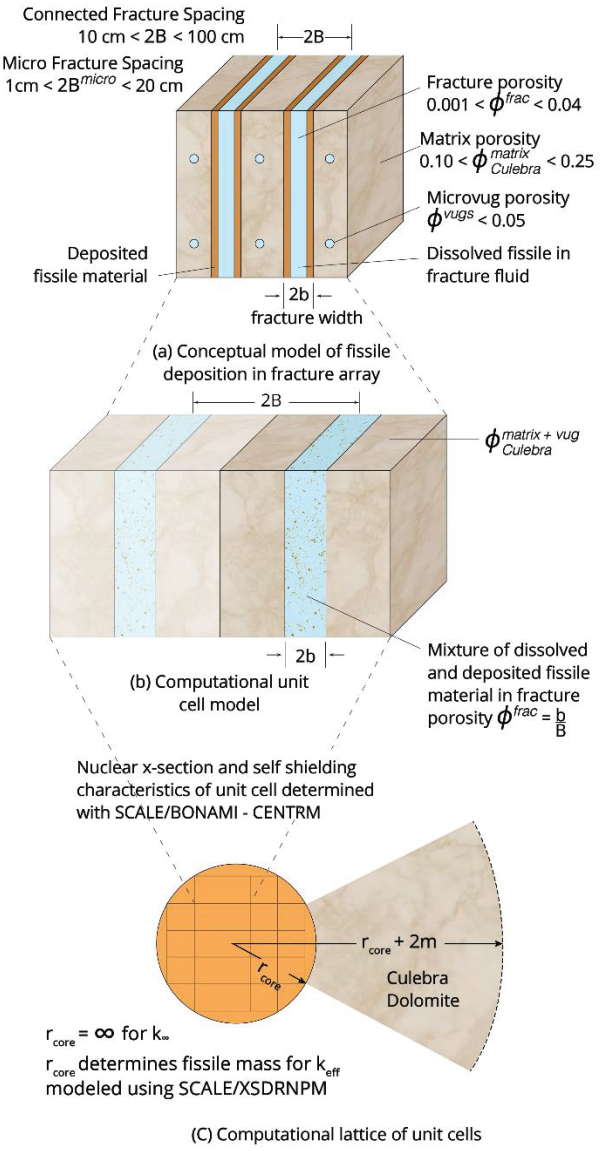


Fig. 24. Heterogeneous conceptual and computational models of fracture deposition in Culebra dolomite. [10, Fig. 22]

These expressions derive from substituting the expression for the total porosity (ϕ^{total}) for the matrix porosity (ϕ^{matrix}_{mat}) and combining the vug and matrix porosity as an equivalent porosity ($\phi^{mat+vug}$) since fissile deposition in the unconnected vugs and matrix was not assumed); specifically,

$$\phi^{matrix}_{mat} \text{ of Eq. (3)} \rightarrow \phi^{total} = \phi^{frac} + \phi^{matrix+vug}(1-\phi^{frac}) \quad (8)$$

$$f^{fissile}_{matrix} \text{ of Eq.(3)} \rightarrow \begin{cases} f^{fissile}_{matrix} \text{ for matrix} \\ f^{fissile}_{frac} \text{ for fracture} \end{cases} \quad (9)$$

The matrix porosity of intact Culebra was varied between 5% and 30%, slightly beyond the measured range (10% < $\phi^{matrix+vug}$ < 25%). The fracture spacing

Information Only

($2B$) was set at 4 or 20 cm in the range of the unconnected micro fractures (1 cm < $2B^{micro}$ < 20 cm). The 20 cm is near the minimum range of connected fracture spacing (10 cm < $2B$ < 100 cm—§II.B.2). The minimum critical radius was set at ~40 cm (Fig. 20) because the planar fracture model would only consist of one fracture with a fracture spacing > 40 cm. The fracture porosity (i.e., ϕ^{frac} = $2b/2B$ where $2b$ is the fracture aperture) was usually set at 1% or bound of 4% ($0.01<\phi^{frac}<1\%$ in §II.B.2).

The nuclear cross-sections for an infinite array of repeating unit cells were processed by the BONAMI and CENTRM modules of SCALE to adjust self-shielding and resonance absorption/flux depressions to include small-scale heterogeneity effects (i.e., include neutron interactions between nearby masses lumped in the fractures). This integral transport capability faithfully models many of the characteristics of Wigner-Seitz cells required to generate volume-averaged cross sections.

At this point, the calculation proceeds in the same manner as the homogeneous calculation using the deterministic XSDRNPM module. Like the finite homogeneous model, the heterogeneous spherical core was surrounded by a spherical reflector of the same Culebra dolomite-brine mixture with a thickness of 2 m (Fig. 24).

VII.B. Plutonium in Culebra Fracture Array

Spacing of a planar fracture array in Culebra dolomite greatly influences the ^{239}Pu minimum critical mass and minimum critical concentration (e.g., minimum critical mass of 3.1 kg for 4-cm fracture spacing versus 90 kg for 20 cm spacing, both at 20% matrix porosity in Fig. 25). At 4-cm fracture spacing, the behavior of the heterogeneous model approaches the behavior of the homogeneous model since the neutron mean free path effectively averages the materials homogeneously.

Fracture porosity determines the maximum mass that may be deposited in a unit volume, provided no fissile deposition occurs in the matrix porosity. For example, the curves terminate at ^{239}Pu density of 101 kg/m^3 when the fracture porosity is filled in Fig. 25. If the fracture porosity was 0.1%, the curves would terminate 10.1 kg/m^3).

As expected from the high concentrations of chloride (Table V), the critical mass in heterogeneous media noticeably increases in Castile brines like homogeneous media (i.e., minimum mass between 6.2 kg and 8.0 kg in Castile brines—Fig. 26—versus minimum mass between 2.8 and 4.7 kg in Culebra brines—Fig. 25).

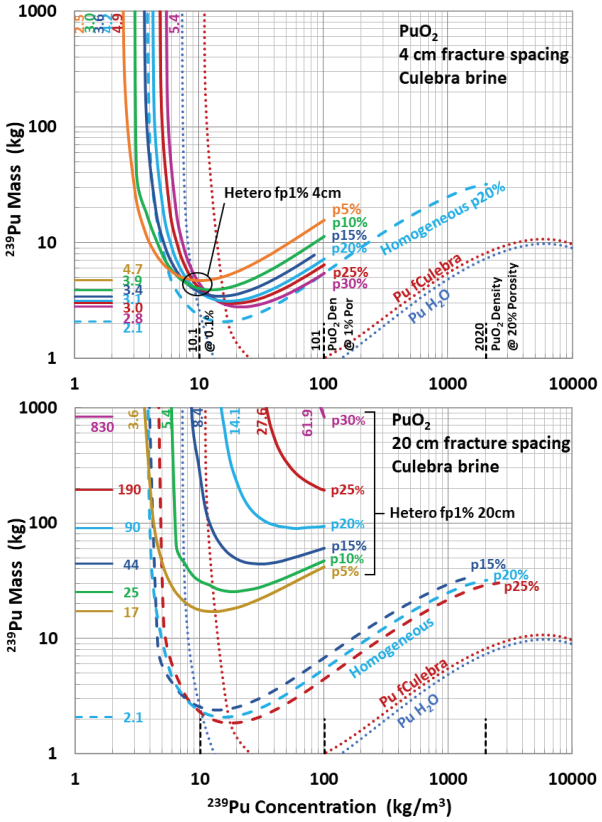


Fig. 25. Critical limits of PuO_2 at variable matrix porosity ($\phi_{Culebra}^{mat+vug}$) with planar fractures saturated with Culebra brine for fracture spacing ($2B$) of 20 and 4 cm and fracture porosity (ϕ^{frac}) of 1% ($2b$ of 0.2 cm and 0.04 cm, respectively).

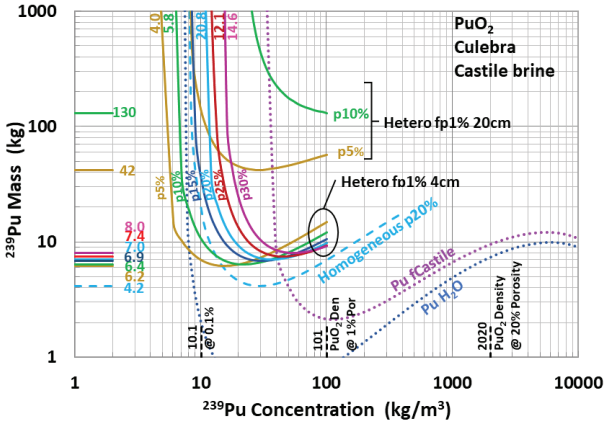


Fig. 26. Critical limits of PuO_2 at variable $\phi_{Culebra}^{mat+vug}$ with planar fractures saturated with Castile brine for $2B$ of 20 and 4 cm and ϕ^{frac} of 1%.

Information Only

VII.C. Uranium in Culebra Fracture Array

Behavior of 93% enriched UO_2 in a Culebra fracture array (Fig. 27) is like that of 100% enriched PuO_2. As previously shown in Fig. 7, the type of U mineral is unimportant at high enrichment; thus, the curves are also applicable to Rutherfordine, UO_2CO_3. Similarly, critical mass noticeably increases in Castile brine versus Culebra brine (Fig. 28).

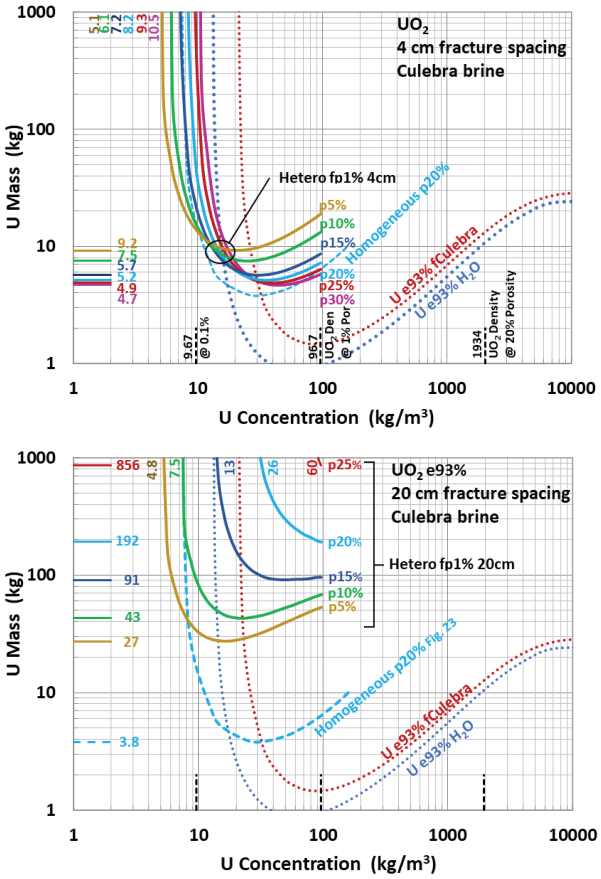


Fig. 27. Critical limits of 93% enriched UO_2 at variable $\phi_{Culebra}^{mat+vug}$ with planar fractures saturated with Culebra brine for $2B$ of 4 and 20 cm and ϕ^{frac} of 1%.

For the highly enriched ^{239}Pu and ^{235}U systems modeled, the critical heterogeneous mass is never less than the saturated homogeneous model if the entire matrix porosity is available for deposition (Fig. 29 and also Fig. 25, Fig. 26, and Fig. 27). Typically, the fracture porosity does not add much to the total porosity. Furthermore, the required mass for criticality in heterogeneous media with only deposition in fractures is larger than in homogeneous media. For example, the maximum pore space for fissile material in a heterogeneous fracture system with deposition only in 1% fracture porosity is 1% while the maximum pore space for fissile material with deposition in the fracture and matrix is between 10% and 25% as shown previously in Fig. 20.

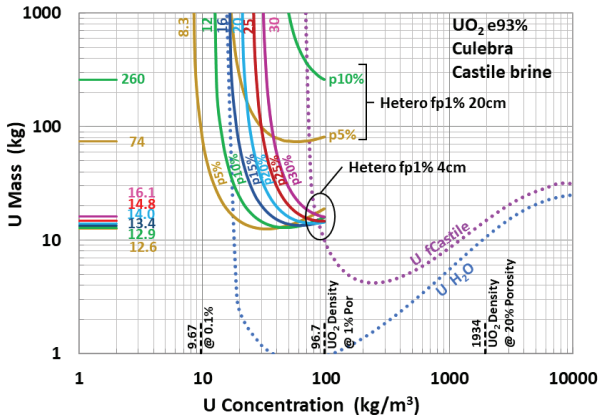


Fig. 28. Critical limits of 93% enriched UO_2 at variable $\phi_{Culebra}^{mat+vug}$ with planar fractures saturated with Castile brine for $2B$ of 4 and 20 cm and ϕ^{frac} of 1%

Similarly, the critical concentration asymptote of the heterogeneous fracture array is never less than a homogenous system provided the porosities correspond. Although only the homogeneous curve at 20% matrix porosity is shown for reference in Fig. 25, Fig. 26, and Fig. 27, if the homogeneous curve at, for example, 5% matrix is plotted, the critical concentration asymptote is less than for the corresponding heterogeneous curve at 5% matrix porosity.

In contrast, a heterogeneous planar fracture system with low enriched uranium, large fracture porosity, and small fracture spacing may be more reactive than a corresponding homogeneous system in Culebra dolomite. For example, a heterogeneous system with 5% ^{235}U enrichment, 4% fracture porosity, and between 0.5 cm and 5 cm fracture spacing is more reactive than a corresponding homogeneous system (Fig. 29. In this situation, the fission neutrons in the fractures can escape the fractures and while slowing down to thermal energies miss the large resonances in the non-fissile isotopes of low enriched fissile material. However, this situation requires fracture porosity and fraction spacing that do not occur in the Culebra dolomite near WIPP. Specifically, the fracture porosity must be at 4%, in the Culebra which is larger than occurs in the Culebra dolomite near WIPP (§II.B.2). Further, the fracture spacing between 0.5 and 5 cm is far smaller than the minimum 10-cm connected fracture spacing that occurs in the Culebra dolomite near WIPP (§II.B.2).

Information Only

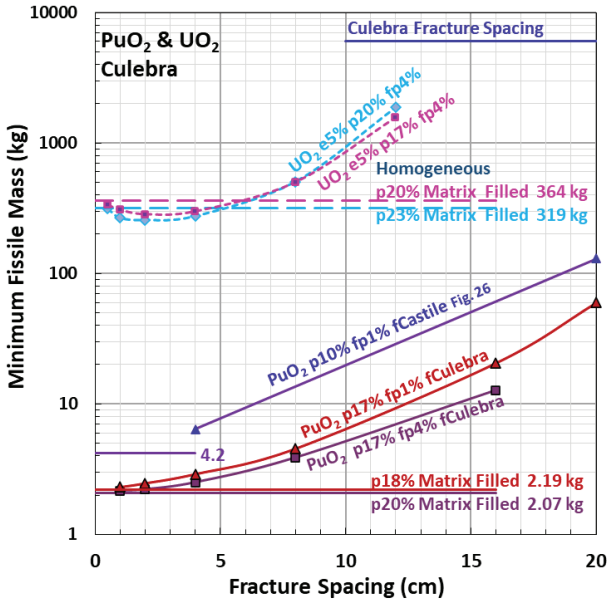


Fig. 29. Influence of fracture spacing on minimum critical mass of highly enriched ^{239}Pu and low enriched ^{235}U in saturated heterogenous Culebra dolomite. [10, Fig. 26]

VII.D. Comparison with Heterogeneous Behavior in Volcanic Tuff

In 1996, Kastenberg et al.[44, 75-77] examined the possibility of an over-moderated, heterogeneous lattice of ^{239}Pu deposited in fractured volcanic tuff becoming supercritical once evaporation initiated criticality. Their tuff fracture model is repeated here as qualitative confirmation of the reasonableness of our Culebra dolomite fracture model. Herein, our analysis is used to examine the possibility of initiating criticality. We are not defending using the static criticality curves to track a transient criticality event.

We also assign the fracture parameters chosen for the volcanic tuff in Culebra dolomite to demonstrate that initiating the critical conditions in a heterogenous system requires larger critical mass than for homogeneous system.

VII.D.1. Fracture System in Volcanic Tuff at Yucca Mountain

Kastenberg et al.[44, 75-77] examined potential criticality consequences in a 2-m diameter deposition of 254 kg ^{239}Pu in fractures spaced (2*B*) 20 cm apart of 1 cm width (2*b*) and 0.5% fracture porosity (as in Fig. 24c). The tuff matrix porosity was 10% in the unsaturated zone of volcanic tuff

Our modeling of the hypothesized static criticality curves in a highly over moderated portion (where moderation is primarily provided by the SiO_2 in the volcanic tuff, not water) is as follows (Fig. 30):[44, Fig. 5] In the first step, sporadic wetting deposits Pu in tuff fractures. The deposit is at the verge of criticality (Step 1: Wet matrix-Wet tuff fractures in a wet heterogeneous configuration with k_{eff} of 1.0 at overall concentration of 6.282 kg/m^3 and mass of 210 kg. At least 41 kg (at 18.8 kg/m^3—0.943 wt. %) must be deposited for the wet fracture system to be critical.

In the second step, evaporation dries the fractures in the unsaturated zone, which makes the configuration subcritical (Step 2: Wet-Dry Hetero with -0.025 difference in k_{eff} between new configuration and critical system at 6.282-kg/m^3 concentration and 210-kg mass of—i.e., Δk_{eff} = -0.025). In the third step, continued evaporation in the unsaturated zone dries out a portion of the matrix (Step 3: 0.5Wet-Dry Hetero with Δk_{eff} of 0.052). In the fourth step, the latter configuration can become critical and thoroughly dry the matrix as positive feedback increases the reactivity (Step 4: Dry-Dry Hetero with Δk_{eff} of 0.015).

In the fifth step of Kastenberg et al,[44, 75-77] criticality with continued positive feedback melts the tuff into a homogeneous mass, because negative temperature feedback does not occur until the tuff reaches temperatures of 1000K. Rather, expansion of the system is the most important negative feedback mechanism at this step (Step 5: Dry Homogeneous with Δk_{eff} of 0.112).

In our analysis, the postulated sequence of static curves is impossible for deposition of <158 kg (at 13.1 kg/m^3—0.659 wt. %). A heterogeneous system can easily go critical between 41-kg PuO_2 and 158-kg PuO_2 during fissile deposition before reaching the unique conditions necessary for auto-catalytic behavior (Fig. 30).

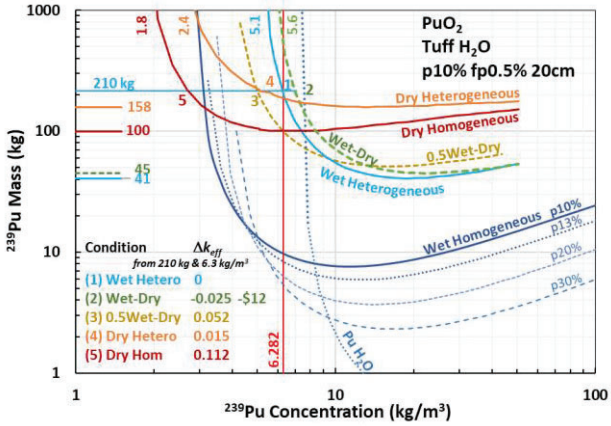


Fig. 30. Heterogeneous fracture system in volcanic tuff with 10% matrix porosity and $^{239}PuO_2$ deposition in 0.5% fracture porosity with 20-cm fracture spacing (10.45% total porosity); water content in matrix set at 100%, 50% and dry; water content in fracture/fissile material set at 100% and dry.

Although masses differ somewhat (Table VII), values of k_{eff} and especially k_{inf} of the static criticality curves match that of Kastenberg et al. static analysis quite well (Table VIII). To elaborate, Kastenberg et al. found that a 2-m sphere was composed of a fracture

Information Only

lattice with 254 kg of ^{239}Pu rather than $^{239}PuO_2$ of 210 kg (17% difference—Table VII) but the multiplication factors were similar; <3% difference for infinite system and <1.8% difference for finite system, except for the dry homogeneous system, which had a 20% difference (Table VII).

Table VII. Comparison of plutonium mass in spherical core in tuff at 10% matrix porosity, 0.5% fracture porosity, 20 cm fracture spacing for current and literature analysis.[44, Table II]

	Mass (kg)		
Radius (m)	Kastenberg	Current	%Δ
1	36.7	48	31
2	254	210	-17
3	794	613	-23
4	1841	1419	-23

Possible reasons for the differences are as follows: Kastenberg et al. performed their analysis with BONAMI-NITAWAL-XSDRN modules and ENDF V cross-sections available in SCALE 4.2 at the time.[44] We used the BONAMI-CENTRM-XSDRNPM modules and ENDF VII available in SCALE 6.1. The CENTRM module of SCALE 6.1 improves processing of resonance absorption/flux depressions by including small-scale heterogeneity effects. Also, ENDF V used 27 neutron cross-section groups while SCALE 6.1 uses 238. Finally, the SiO_2 cross-sections in ENDF V changed substantially in ENDF VII. The cross-sections have much finer energy resolution and the SiO_2 is represented by all its isotopes rather than a single element cross-section set.

Table VIII. Comparison of multiplication factor and reactivity in current with literature analysis for several static conditions of moisture in volcanic tuff fractures at 100% and 95.5% enrichment for ^{239}Pu and $^{239}PuO_2$.

		Wet Fracture		0.9 Wet Fracture		0.75 Wet Fracture		0.5 Wet Fracture		Dry Fracture		Dry Homogeneous	
Tuff System[a]	Enrich	Multi Factor	Rel React	Multi Factor	Rel React	Multi Factor	Rel React	Multi Factor	Rel React	Multi Factor	Rel React	Multi Factor	Rel React
Infinite	(%)	(k_{inf})	($)	(k_{inf})	($)	(k_{inf})	($)	(k_{inf})	($)	(k_{inf})	($)	(k_{inf})	($)
Kastenberg[b]		0.98	-9.4	0.99	-4.7	1.01	4.7	1.06	28	1.22	104	1.34	160
Pu	100	0.973	-12.7	0.994	-2.8	1.029	13.7	1.090	42	1.226	107	1.344	162
PuO_2	100	0.974	-12.3					1.092	43	1.227	107	1.345	163
Pu	95.5	0.976	-11.3					1.079	37	1.123	58	1.149	70
PuO_2	95.5	0.977	-10.8					1.080	38	1.124	58	1.149	70
Finite	(%)	(k_{eff})	($)	(k_{eff})	($)	(k_{eff})	($)	(k_{eff})	($)	(k_{eff})	($)	(k_{eff})	($)
Kastenberg[b]		0.99	-4.7	1.00	0.0	1.01	4.7	1.04	19	1.025	12	1.35	165
Pu	100	0.973	-12.7	0.990	-4.7	1.04	18.9	1.050	24	1.013	6	1.111	52
PuO_2	100	0.975	-11.8					1.052	25	1.015	7	1.112	53

[a] Tuff porosity 10%, fracture porosity 0.5%, fracture spacing 20 cm.
[b] Estimated from Figures[44, Figs. 6&9]

At high enrichment, the mineral form (i.e., Pu or PuO_2) has only small influence on the multiplication factor (k_{inf} or k_{eff}) and reactivity (Table VIII), as can also be surmised for uranium in Fig. 8. As to be expected, however, the enrichment has more influence. For 95.5% enrichment (about one-half of the initial and final ^{239}Pu enrichment in RPPCR-23-19P and CRA-26-19P—Table I), the difference from 100% enrichment for an infinite system is ~10% for a wet matrix/wet fracture but increases to a difference of ~60% for a dry homogeneous system.

VII.D.2. Fracture System in Culebra Dolomite using Volcanic Tuff Fracture Parameters

The 0.5% fracture porosity and 20 cm fracture spacing in the volcanic tuff could apply to the Culebra dolomite at WIPP although the 10% matrix porosity is at the distribution minimum. There are several ways to identify a comparable situation in the Culebra. Here, we select the same 2-m fissile diameter. The corresponding mass is 314 kg at concentration of 7.4 kg/m^3 at Step 1 (Fig. 31).[j]

At least 31 kg (at 24.3 kg/m^3—0.954 wt. %—Fig. 31) must be deposited for the wet heterogeneous Culebra fracture system to be critical, which is somewhat less than the 41 kg PuO_2 in volcanic tuff (Fig. 30). The heterogeneous PuO_2 assembly in dry Culebra dolomite is also more reactive than the dry volcanic tuff: 6.7 kg

[j] Other comparable situations would be to equate in the two systems (a) overall 6.282 kg/m^3 fissile concentration, or (b) 210-kg fissile mass.

Information Only

versus 100 kg for dry homogeneous system and 19 kg versus 158 kg for dry heterogenous system (Fig. 31 and Fig. 30, respectively).

Although the same sequence of events can be postulated, the fissile assembly at WIPP is in the saturated zone and thus a critical event is necessary to initiate dry out in second step (rather than evaporation as possible in unsaturated zone in tuff)[k] (Step 2: Wet-Dry Hetero with k_{eff} of 0.980 at mass of 314 kg). The ability of the system to move past Step 2 when the system goes subcritical is improbable in the saturated zone, because of the negative reactivity of -9.6$ (i.e., 9.6$= $(k_{eff}-1)/\beta$ where β is the fraction of delayed neutrons which is 0.00212 for ^{239}Pu fission). For comparison, shutdown reactivities for large commercial reactors are -5.7$ for boiling water reactors, -4.3$ for pressure water reactors, 4.0$ for high temperature gas reactors, and -11.2$ for a liquid-metal, fast reactor with ^{239}Pu.[59]

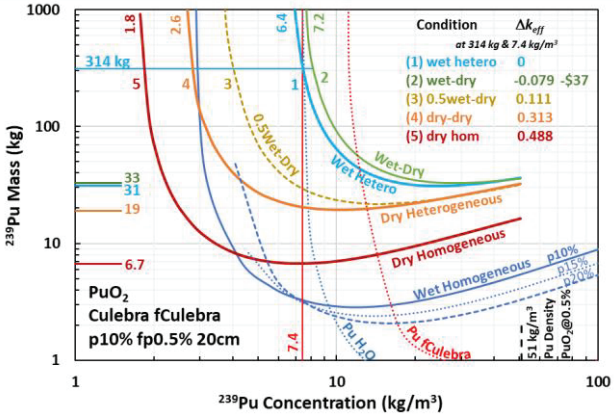


Fig. 31. Heterogeneous fracture system in Culebra dolomite with 10% matrix/vug porosity, and $^{239}PuO_2$ deposition in 0.5% fracture porosity with 20-cm fracture spacing (10.45% total porosity); Culebra brine content in matrix set at 100%, 50% and dry; brine content in fracture/fissile material set at 100% and dry.

For a matrix porosity of 17%, which is near the Culebra mean and median of 16% ($10\% < \phi_{Culebra}^{matrix+vug} < 25\%$—§II.B.2), maximum fracture porosity of 1% ($0.01\% < \phi_{Culebra}^{frac} < 1\%$—§II.B.2), and fracture spacing of 20 cm ($10\text{ cm} < 2B < 100\text{ cm}$—§II.B.2), the same sequence can be postulated. The negative insertion reactivity is still large for Step 2, which will shut down the criticality (Fig. 32).

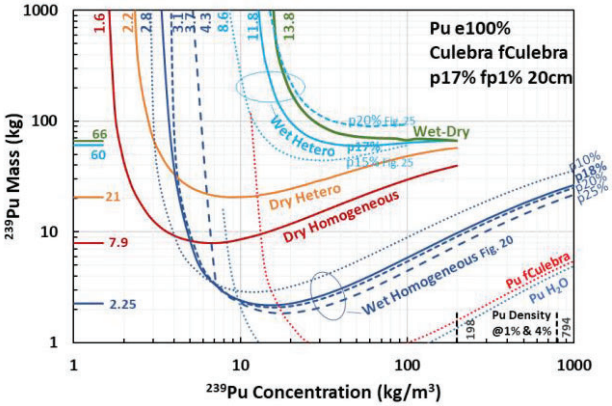


Fig. 32. Heterogeneous fracture system in 17% matrix/vug porosity with ^{239}Pu deposition in 1% and 4% fracture porosity and 20 cm fracture spacing.

In Fig. 31 and Fig. 32, the dry homogeneous system critical limits are similar but not identical in each analysis because the matrix porosity differs. The matrix porosity causes a slight change in the mass of moderating dolomite present. The matrix porosity is much less important in a dry system than in a wet homogeneous system because the porosity does not contain the moderating H_2O or WIPP brine.

VIII. CONCLUSIONS

VIII.A. Geologic Media Increases Critical Mass but often Decreases Critical Concentration

In general, the addition of geologic media to a fissile/water binary system substantially increases the mass of fissile material necessary to go critical for ^{239}Pu (Fig. 33) and ^{235}U. In salt, the mass of 5% uranium required almost exceeds the anticipated uranium mass to be placed in WIPP. The exception is hydrated montmorillonite clay with sufficient bound water present such that the fissile material is highly moderated even in the presence of clay components Si_4O_{10} and $Al_2(OH)_6$.

The influence of geologic media on the asymptotic concentration varies. For geologic material primarily composed of elements with large neutron absorption cross-sections in the thermal region such as iron in rust or chloride in salt, the geologic material increases the concentration asymptote compared to fissile/water binary system (Fig. 33).

[k] Drawdown from a water well is not considered.[44, p.304] EPA narrowed the focus of regulatory interest of human disruptions of the WIPP disposal system to[78] (a) fluid injection into repository from for deep oil recovery outside legislated WIPP LWA,[21] (b) seepage and subsidence from oil and gas well development outside LWA, (c) subsidence in aquifers above repository from potash mining outside LWA, and (d) exploratory boreholes for resources (which usually bypass the Salado natural barrier). Speculative long-term human disruptions, such as long-term use of water wells in the legislated LWA that bypass much of the Culebra dolomite natural barrier, are not required.[20, 78]

Information Only

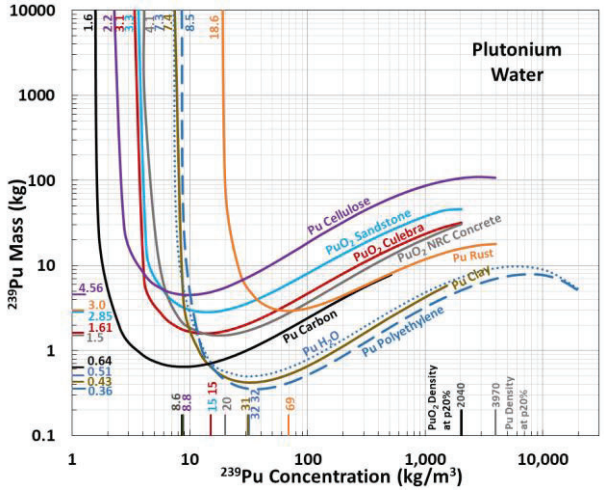


Fig. 33. Critical limits for 100% enriched ^{239}Pu and $^{239}PuO_2$ deposited as sphere in various homogeneous material at 20% total porosity saturated with water. [10, Fig. 27]

For geologic material primarily composed of elements with small thermal absorption cross-sections such as silicon, the geologic material decreases the critical concentration. Specifically, the minimum concentration and mass in sandstone and volcanic tuff are similar because of the dominate influence of SiO_2 thermal neutron absorptive cross-sections (84% and 77% when oxidized to SiO_2—Table III). Also, critical concentrations of Culebra dolomite are similar to sandstone because of the similar thermal neutron absorption cross-sections of Ca^{+2} and Mg^{+2} (91.5%). Finally, NRC-concrete, which is also composed of elements with similar thermal neutron absorption cross-sections (SiO_2 with some CaO and Al_2O_3—Table III) behaves similarly (particularly like Culebra dolomite).

The behavior of 93% enriched UO_2 is similar to 100% enriched PuO_2 (Fig. 34). For 5% enriched UO_2, however, the total mass of uranium is a U-shaped curve that increases exponentially when over moderated and under moderated (Fig. 34). Large masses and concentrations are usually required for low enriched ^{235}U.

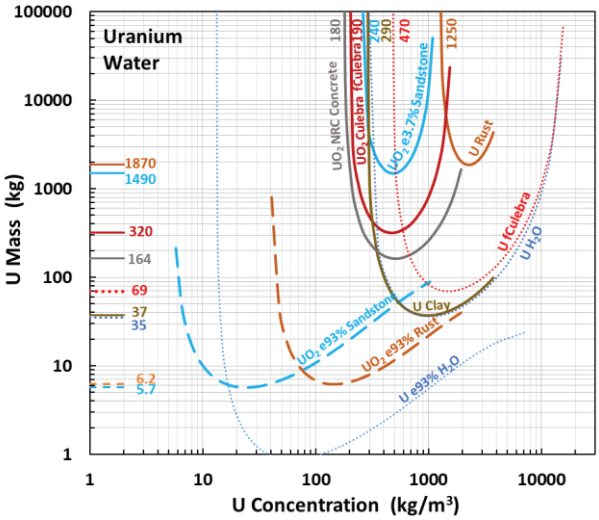


Fig. 34. Criticality limits for 5% and 93% enriched U and UO_2 deposited as sphere in various homogeneous material at 20% total porosity with water and Culebra brine.

VIII.B. Brine Fluids Increase Critical Limits

The substitution of WIPP brines for water in a fissile/fluid binary system substantially increases the critical mass and moderately increases the asymptotic concentration necessary to go critical for ^{239}Pu (Fig. 35) and ^{235}U (Fig. 36).

The corresponding critical spherical radius for 100% enriched PuO_2 (and UO_2 at high enrichment) in various material and fluids somewhat plateaus between 100 and 1000 kg/m^3 (Fig. 37) but does not have a minimum until the porosity is filled. In contrast, UO_2 at 5% enrichment in various material and fluids have minimums that place geometric constraints on criticality (Fig. 38).

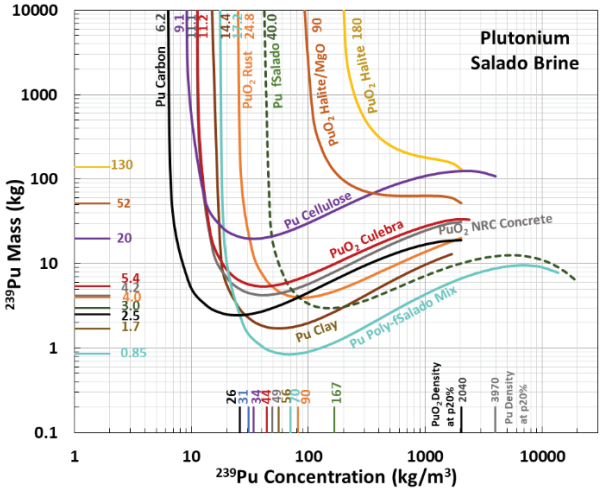


Fig. 35. WIPP Salado brine substantially increases most critical limits for ^{239}Pu and $^{239}PuO_2$ deposited as sphere in various homogenous materials with 20% total porosity. [10, Fig. 28]

Information Only

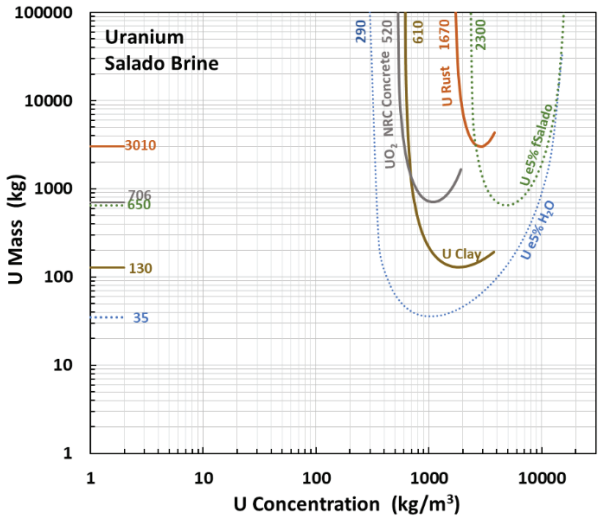


Fig. 36. Salado brine increases critical limits for U and UO_2 at 5% enrichment deposited as sphere in various homogeneous materials with 20% porosity.

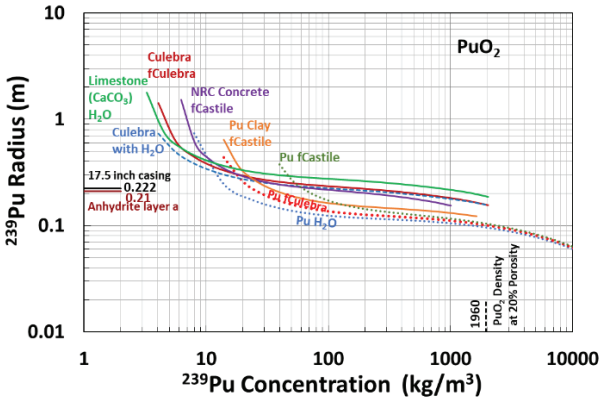


Fig. 37. Critical radius for PuO_2 in various media with 20% porosity filled with water and WIPP brines

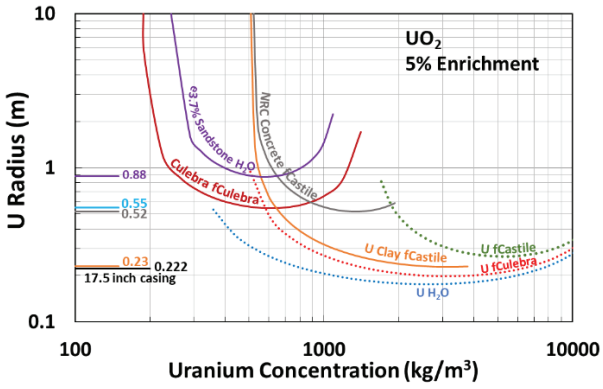


Fig. 38. Critical radius for UO_2 in various media with 20% porosity filled with water and WIPP brines

VIII.C. Porosity Influences Critical Mass and Concentration.

The matrix porosity of homogeneous geologic media has a strong influence on both the critical mass and the critical concentration in brine and water. As the porosity increases, the behavior approaches that of a fissile/fluid binary system, and the critical mass usually decreases. However, carbon material with water and NRC concrete with Salado brine are exceptions (Fig. 39). With carbon material, the carbon is slightly more effective than water as a moderator at low porosities. In the situation with NRC concrete (without Mg and with only SiO_2), the Cl^{-1} in the Salado brine increases the critical fissile mass as the matrix porosity increases at low porosities.

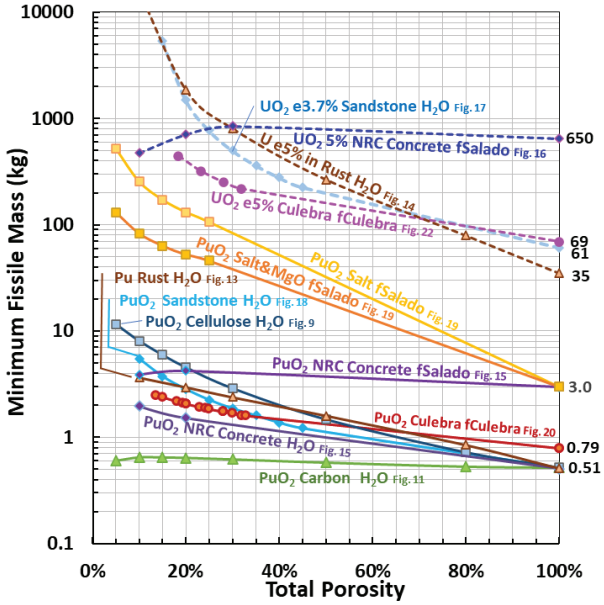


Fig. 39. Critical mass usually decreases with increase in material porosity because influence of homogeneous media on reactivity decreases.[10, Fig. 29]

The influence of porosity on the concentration asymptote depends on whether the geologic material has chemical elements with small neutron absorption cross-sections in the thermal region, or elements with large neutron absorption in the thermal region (Fig. 40). With small neutron absorption cross-sections, such as Mg^{+2} and Ca^{+2} in Culebra dolomite the concentration asymptote increases when porosity increases. With large neutron absorption in the thermal region, such as Cl^{-1} in halite or Fe^{+3} or Fe^{+4} in rust, the concentration asymptote decreases when porosity increases (Fig. 40).

VIII.D. Fracture Spacing in Culebra Influences Critical Limits

The Culebra dolomite is most accurately modeled as fractured heterogeneous media with deposition primarily limited to the fractures. In both homogeneous and

Information Only

heterogeneous fracture systems, matrix porosity influences both the minimum mass (Fig. 41) and the concentration asymptote (Fig. 42). Furthermore, spacing of fracture heterogeneity greatly influences the fissile minimum critical mass (Fig. 41) and minimum critical concentration (Fig. 42).

As expected from high concentrations of Cl^{-1} (Table V and Fig. 4), the critical mass and concentration noticeably increases for Castile brine (Fig. 41 and Fig. 42).

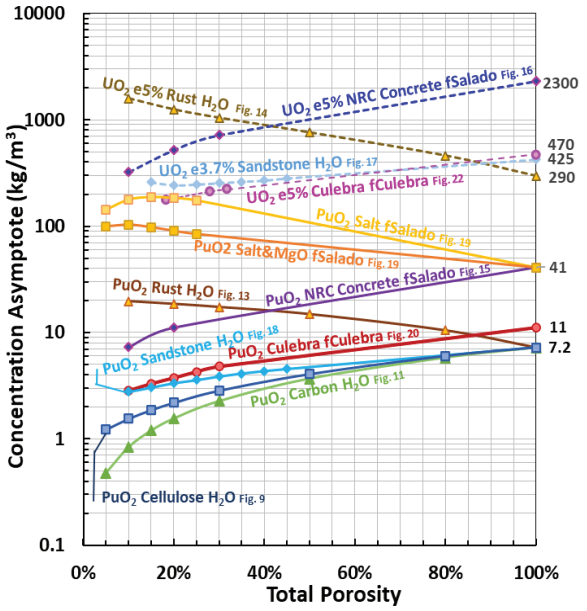


Fig. 40. Concentration asymptote increases with porosity for media with small thermal neutron absorbing cross-sections, such as Culebra dolomite, and decreases with porosity for media with large thermal cross-sections, such as halite and rust.[10, Fig. 30]

Fracture porosity has much less influence than either matrix porosity or fracture spacing (i.e., the minimum critical mass at low total porosity is similar for fracture porosity of 0.1%, 1%, and 4%). However, fracture porosity determines the maximum mass that may be deposited in a unit volume, provided no fissile deposition occurs in the matrix porosity. A homogeneous model with ^{239}Pu or highly enriched ^{235}U bounds both the minimum critical concentration and mass of a heterogeneous model (Fig. 41 and Fig. 42).

VIII.E. Summary

The mass of fissile material collected in a region of geologic media is dependent on elapsed time for deposition unless geometrical constraints exist on the space available. In contrast, the asymptotic criticality concentration limits calculated here for an infinite media system are most often used in companion reports to demonstrate the lack of criticality concern for two reasons: Concentration limits are (1) independent of elapsed time, and (2) more readily compared to geologic processes such as precipitation, sorption, and colloidal aggregation/filtration. The criticality limits in geologic media are useful for demonstrating the low probability of criticality in the bedded salt disposal system after closure when humans are absent. The limits are not for evaluating nuclear criticality safety during repository operations or transportation of fissile material when humans are present.

Information Only

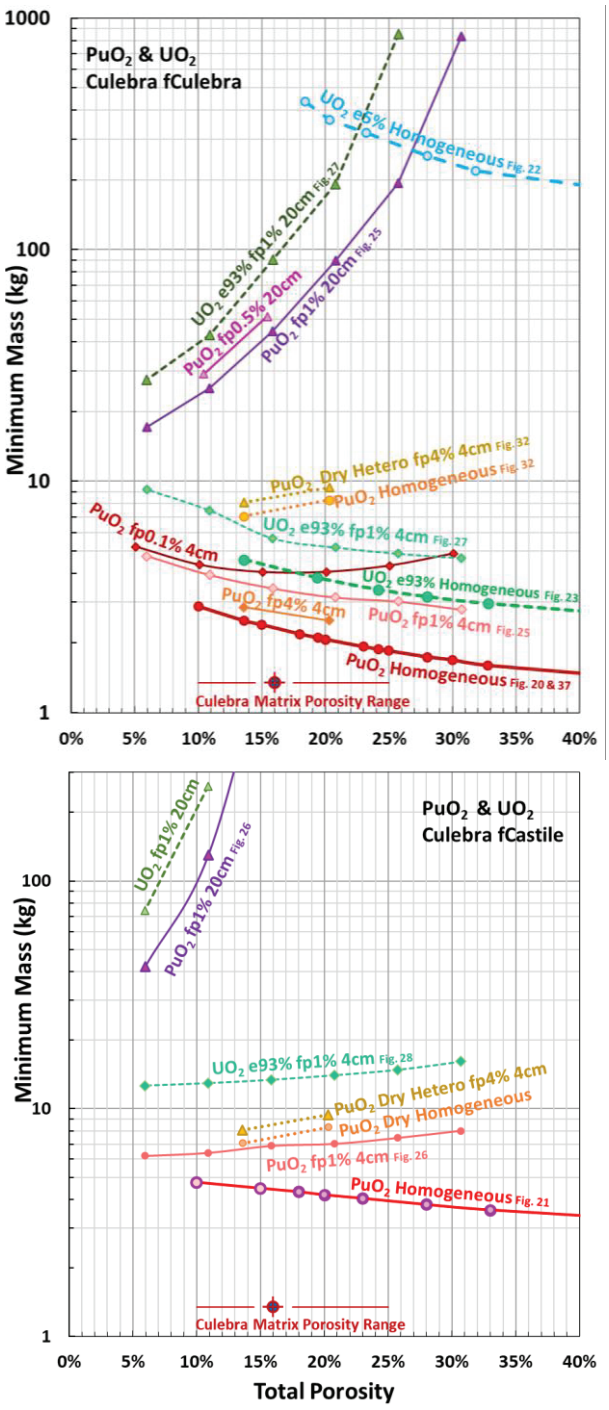


Fig. 41. Critical mass of 100% enriched ^{239}Pu and 93% enriched ^{235}U for homogeneous models in Culebra dolomite less than for heterogeneous models for both Culebra and Castile brines.

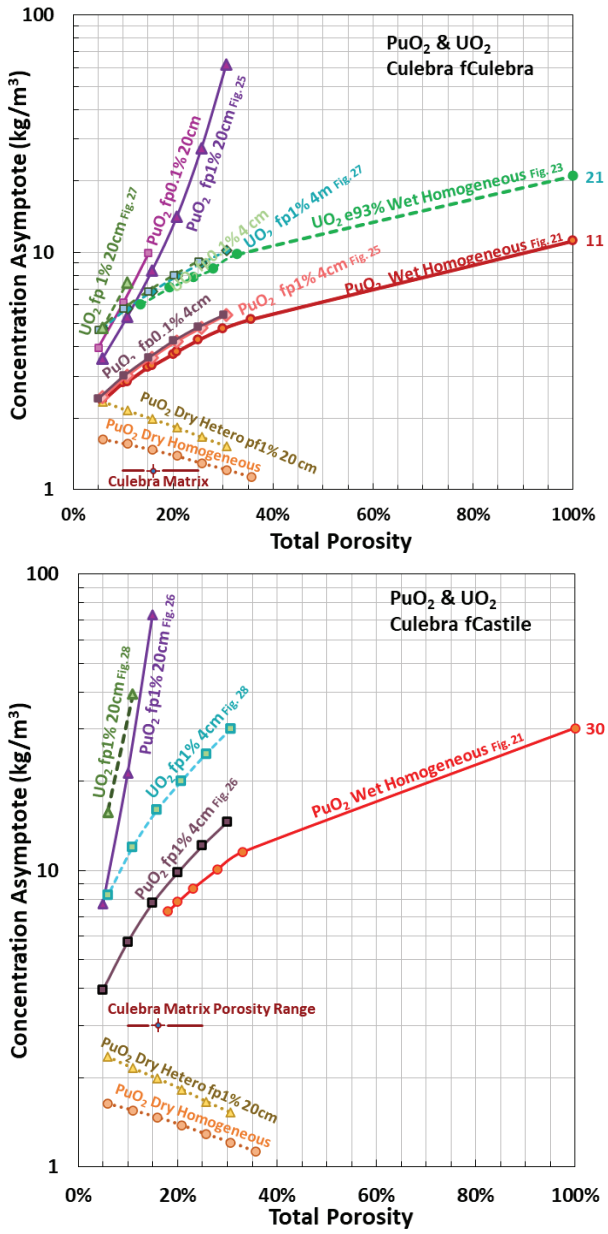


Fig. 42. Critical concentration asymptote of 100% enriched ^{239}Pu and 93% enriched ^{235}U influenced by matrix porosity, pore fluid type, and fracture spacing in Culebra dolomite.

Information Only

REFERENCES

1. R. P. RECHARD, L. C. SANCHEZ, H. R. TRELLUE, and C. T. STOCKMAN, "Unfavorable Conditions for Nuclear Criticality Following Disposal of Transuranic Waste at the Waste Isolation Pilot Plant," *Nuclear Technology,* **136**, 1, 99–129 (2001).
2. R. P. RECHARD, L. C. SANCHEZ, C. T. STOCKMAN, and H. R. TRELLUE, "Consideration of Nuclear Criticality When Disposing of Transuranic Waste at the Waste Isolation Pilot Plant," SAND99-2898, Sandia National Laboratories, (2000).
3. R. P. RECHARD, "Probability and Consequences of Nuclear Criticality at a Geologic Repository--I: Conceptual Overview for Screening," *Nuclear Technology,* **190**, 2, 97–126 (2015).
4. DOE (US DEPARTMENT OF ENERGY), "Surplus Plutonium Disposition, Record of Decision," *Federal Register,* **81**, 65, 19588–19594 (2016).
5. DOE (US DEPARTMENT OF ENERGY), "Title 40 CFR Part 191 Compliance Recertification Application for the Waste Isolation Pilot Plant," DOE/WIPP-10-3609, Carlsbad Area Office, US Department of Energy, (2019).
6. S. BRUNELL, J. BETHUNE, P. DOCHERTY, D. C. KICKER, S. KIM, S. KING, J. LONG, and T. R. ZEITLER, "Summary Report for the 2023 Replacement Panels Planned Change Request Performance Assessment," ERMS 579729, Sandia National Laboratories, (2023).
7. DOE (US DEPARTMENT OF ENERGY), "Notice of Availability of Final Environmental Impact Statement for Surplus Plutonium Disposition Program," *Federal Register,* **89**, 13, 3642–3644 (2024).
8. NA/NRC (NATIONAL ACADEMIES/NATIONAL RESEARCH COUNCIL), "Review of the Department of Energy's Plans for Disposal of Surplus Plutonium in the Waste Isolation Pilot Plant," The National Academies Press, (2020).
9. R. P. RECHARD, L. C. SANCHEZ, P. J. MCDANIEL, J. HUNT, and G. BROADOUS, "Fissile Mass and Concentration Criteria in Geologic Media near Bedded Salt Repository " International High-Level Radioactive Waste Management Conference, April 14-18, 2019, Knoxville, TN, (2019).
10. R. P. RECHARD, L. C. SANCHEZ, M. OLGVUN, and G. RYBA, "Fissile Mass and Concentration Necessary for Criticality in Geologic Media near Bedded Salt Repository, Memorandum to Paul E. Shoemaker, 8880; Todd Zeitler, 8862; Ross Kirkes, 8883; November 2019," Sandia National Laboratory, (2019).
11. R. P. RECHARD and E. STEIN, "Hydrologic and Geochemical Constraints on Criticality in Geologic Media near Bedded Salt Repository; Memorandum to Paul E. Shoemaker, 8880; Todd Zeitler, 8863; Ross Kirkes, 8883; November 2019," Sandia National Laboratories, (2019).
12. R. P. RECHARD, S. KING, and P. V. BRADY, "Hydrologic and Geochemical Constraints on Post-Closure Criticality in Geologic Media near Waste Isolation Pilot Plant," SAND2025, Sandia National Laboratories, (2025).
13. R. P. RECHARD, B. A. DAY, B. REEDLUNN, and J. E. BEAN, JR., "Improbability of Nuclear Criticality in Criticality Control Overpacks after Salt Creep Compaction at Waste Isolation Pilot Plant," SAND2022-0952, Sandia National Laboratories, (2022).
14. R. P. RECHARD, B. A. DAY, B. REEDLUNN, and J. E. BEAN, JR., "Improbability of Post-Closure Criticality in Compacted Criticality Control Overpacks after Room Closure at Waste Isolation Pilot Plant," SAND2025, Sandia National Laboratories, (2025).
15. R. P. RECHARD, "Improbability of Transuranic Waste Compaction by Salt Creep Causing Criticality in Bedded Salt Repository; Memorandum to Paul E. Shoemaker, 8880; Todd Zeitler, 8863; Ross Kirkes, 8883; November 2019," Sandia National Laboratories, (2019).
16. R. P. RECHARD, B. REEDLUNN, J. E. BEAN, JR., B. A. DAY, and L. C. SANCHEZ, "Improbability of Post-Closure Criticality in Array of Transuranic Waste Containers after Compaction by Salt Creep at Waste Isolation Pilot Plant," SAND2025, Sandia National Laboratories, (2025).
17. R. P. RECHARD, "Low Risk of Post-Closure Criticality at Waste Isolation Pilot Plant " SAND2025, Sandia National Laboratories, (2025).
18. E. D. CLAYTON, "Anomalies of Nuclear Criticality," PNNL-19176, Pacific Northwest National Laboratory, (2010).
19. EPA (US ENVIRONMENTAL PROTECTION AGENCY), "40 CFR Part 191: Environmental Standards for the Management and Disposal of Spent Nuclear Fuel, High-Level and Transuranic Radioactive Wastes: Final Rule," *Federal Register,* **50**, 182, No. 182, 38066–38089 (1985).
20. EPA (US ENVIRONMENTAL PROTECTION AGENCY), "40 CFR Part 191: Environmental Radiation Protection Standards for the Management and Disposal of Spent Nuclear Fuel, High-Level and Transuranic Radioactive Wastes, Final Rule," *Federal Register,* **58**, 242, 66398–66416 (1993).
21. PUB. L. 102-579, *Waste Isolation Pilot Plant Land Withdrawal Act*, 106 Stat. 4777, (1992).
22. G. D. VAN SOEST, "Performance Assessment Inventory Report - 2018," INV-PA-18, Revision 0, Los Alamos National Laboratory, (2018).
23. G. D. VAN SOEST, "Performance Assessment Inventory Report - 2022," INV-PA-22, Revision 0, Los Alamos National Laboratory, (2022).
24. D. C. KICKER, "Radionuclide Inventory Screening Analysis for the Replacement Panels Planned Change Request Performance Assessment (RPPCR PA)," ERMS 578878, Sandia National Laboratories, (2023).
25. G. D. VAN SOEST, "Full Repository Performance Assessment Inventory Report - 2024," INV-FPA-24, Los Alamos National Laboratory, (2025).
26. H. K. CLARK, "Subcritical Limits for Plutonium Systems," *Nuclear Science and Engineering,* **79**, 1, 65–84 (1981), doi: 10.13182/NSE81-A19043.

Information Only

27. ANSI (AMERICAN NATIONAL STANDARDS INSTITUTE), "An American National Standard for Nuclear Criticality Safety in Operations with Fissionable Materials Outside Reactors," ANSI/ANS-8.1-2014, American National Standards Institute, (2014).
28. T. R. ZEITLER, J. BETHUNE, S. BRUNELL, P. DOCHERTY, S. KIM, S. KING, and J. WILGUS, "Analysis Report for 12-Panel PA Sensitivity Study," Sandia National Laboratories, (2025).
29. EPA (US ENVIRONMENTAL PROTECTION AGENCY), "EPA Review of Doe Replacement Panels Planned Change Request, Part 1: Review of Doe 12-Panel Sensitivity Study," US Environmental Protection Agency, Office of Radiation and Indoor Air, (2025).
30. C. L. STEIN, "Mineralogy in the Waste Isolation Pilot Plant (WIPP) Facility Stratigraphic Horizon," SAND85-0321, Sandia National Laboratories, (1985).
31. M. G. MARIETTA, D. R. ANDERSON, G. BASABILVAZO, J. C. HELTON, and H.-N. JOW, "Summary Discussion of the 1996 Performance Assessment for the Waste Isolation Pilot Plant," *Reliability Engineering and System Safety,* **69**, 1-3, 437–452 (2000).
32. R. P. RECHARD, "Historical Background on Performance Assessment for the Waste Isolation Pilot Plant," *Reliability Engineering and System Safety,* **69**, 1-3, 5–46 (2000).
33. L. C. MEIGS, R. L. BEAUHEIM, J. T. MCCORD, Y. W. TSANG, and R. HAGGERTY, "Design, Modelling, and Current Interpretations of the H-19 and H-11 Tracer Tests at the Wipp Site," Field Transport Experiments: Role in the Prediction of Radionuclide Migration: Synthesis and Proceeding of an NEA/EC GEOTRAP Workshop, Cologne, Germany, August 28–30, 1996pp. 157–169 (1996).
34. R. S. E. CARMICHAEL, *CRC Handbook of Physical Properties of Rocks, Vol. III.* Boca Raton, FL: CRC Press, Inc., 1984.
35. S. P. CLARK, *Handbook of Physical Constants*. New York, NY: Geological Society of America, Inc., 1966.
36. A. SHAKOOR and H. R. HUME, "Chapter 3: Mechanical Properties," in *Physical Properties Data for Rock Salt*. Washington, DC: National Bureau of Standards, 1981.
37. R. D. KRIEG, "Reference Stratigraphy and Rock Properties for the Waste Isolation Pilot Plant (Wipp) Project," SAND83-1908, Sandia National Laboratories, (1984).
38. M. D. SIEGEL, S. J. LAMBERT, and K. L. ROBINSON, "Hydrogeolchemical Studies of the Rustler Formation and Related Rocks in the Waste Isolation Pilot Plant Area, Southeastern New Mexico," SAND88-0196, Sandia National Laboratories, (1991).
39. L. H. BRUSH, "Test Plan for Laboratory and Modeling Studies of Repository and Radionuclide Chemistry for the Waste Isolation Pilot Plant," SAND90-0266, Sandia National Laboratories, (1990).
40. R. P. RECHARD, "Historical Background on Assessing the Performance of the Waste Isolation Pilot Plant," SAND98-2708, Sandia National Laboratories, (1999).
41. T. SEWARDS, A. BREARLEY, R. GLEN, I. D. R. MACKINNON, and M. D. SIEGEL, "Nature and Genesis of Clay Minerals of the Rustler Formation in the Vicinity of the Waste Isolation Pilot Plant in Southeastern New Mexico," SAND90-2569, Sandia National Laboratories, (1992).
42. E. M. SAYLOR and J. M. SCAGLIONE, "Nuclear Criticality Safety Assessment of Potential Plutonium Disposition at the Waste Isolation Pilot Plant," ORNL/TM-2017/751/R1, Oak Ridge National Laboratory, (2018).
43. F. GAUTHIER-LAFAYE, F. WEBER, and H. OHMOTO, "Natural Fission Reactors of Oklo," *Economic Geology,* **84**, 8, 2286 (1989).
44. W. E. KASTENBERG, P. F. PETERSON, J. AHN, J. BURCH, G. CASHER, P. L. CHAMBRÉ, E. GREENSPAN, D. R. OLANDER, J. L. VUJIC, B. BESSINGER, N. G. W. COOK, F. M. DOYLE, and L. B. HILBERT, "Considerations of Autocatalytic Criticality of Fissile Materials in Geologic Repositories," *Nuclear Technology* **115**, 3, 298–310 (1996).
45. P. C. GOODELL, "Geology of the Peña Blanca Uranium Deposits, Chihuahua, Mexico. Uranium in Volcanic and Volcaniclastic Rocks," *AAPG Studies in Geology. American Association of Petroleum Geologists,* No. 13, 275 (1981).
46. D. E. BROXTON, R. G. WARREN, R. C. HAGAN, and G. LUEDERMANN, "Chemistry of Diagenetically Altered Tuffs at a Potential Nuclear Waste Repository, Yucca Mountain, Nye County, Nevada," LA-10802-MS, Los Alamos National Laboratory, (1986).
47. DOE (US DEPARTMENT OF ENERGY), "Title 40 Cfr Part 191: Compliance Certification Application for the Waste Isolation Pilot Plant," DOE/CAO-1996-2184. Vol. I-XXI, DOE Carlsbad Area Office, (1996).
48. R. P. RECHARD, A. C. PETERSON, J. D. SCHREIBER, H. J. IUZZOLINO, M. S. TIERNEY, and J. S. SANDHA, "Preliminary Comparison with 40 CFR Part 191, Subpart B for the Waste Isolation Pilot Plant, December 1991, Volume 3: Reference Data," SAND91-0893/3, Sandia National Laboratories (1991).
49. R. P. RECHARD and M. S. TIERNEY, "Assignment of Probability Distributions for Parameters in the 1996 Performance Assessment for the Waste Isolation Pilot Plant, Part 2: Application of Process," *Reliability Engineering and System Safety,* **88**, 1, 33–80 (2005).
50. D. E. DEAL, R. J. ABITZ, D. S. BELSKI, J. B. CASE, M. E. CRAWLEY, C. A. GIVENS, P. P. J. LIPPONNER, D. J. MILLIGAN, J. MYERS, D. W. POWERS, and M. A. VALDIVIA, "Brine Sampling and Evaluation Program, 1992-1993 Report and Summary of Bsep Data since 1982," (1995).
51. J. L. KRUMHANSL, K. M. KIMBALL, and C. L. STEIN, "Intergranular Fluid Compositions from the Waste Isolation Pilot Plant (WIPP), Southeastern New Mexico," SAND90-584, Sandia National Laboratories, (1991).
52. P. S. DOMSKI, "Prediction of Baseline Actinide Solubilities for the Replacement Panels Planned Change Request (RPPCR) Performance Assessment," ERMS 555726, Sandia National Laboratories, (2023).

Information Only

53. R. S. POPIELAK, R. L. BEAUHEIM, S. R. BLACK, W. E. COONS, C. T. ELLINGSON, and R. L. OLSEN, "Brine Reservoirs in the Castile Formation, Waste Isolation Pilot Plant Project, Sourtheastern New Mexico," TME 3153, U.S. Department of Energy, WIPP Project Office, (1983.).
54. L. H. BRUSH and P. S. DOMSKI, "Prediction of Baseline Actinide Solubilities for the WIPP CRA-2014 PA," AP-153, Rev. 1 records package, Sandia National Laboratories, (2014).
55. H. W. PAPENGUTH and Y. K. BEHL, "Test Plan: Evaluation of Dissolved Actinide Retardation at the Waste Isolation Pilot Plant," TP 96-02. WPO 31336, Sandia National Laboratories, (1996).
56. P. S. DOMSKI, "Prediction of Baseline Actinide Solubilities for the 2026 Wipp Compliance Recertification Performance Assessment Final-State Analysis (Cra-2026 Fs)," ERMS, Sandia National Laboratories, (2025).
57. P. J. MCDANIEL, J. M. HARRIS, and D. H. WIDMAN, "A Theoretical Analysis of the Effect of Thermal Neutron Absorbers on Dual-Detector Porosity Log Measurements," 24th Annual Logging Symposium, June 27-30, 1983, Paper LL, (1983).
58. ORNL (OAK RIDGE NATIONAL LABORATORY), "Scale Code System," ORNL/TM-2005/39, Version 6.2.1, Oak Ridge National Laboratory. Most recent version available from Radiation Safety Information Computational Center as CCC-834.
59. J. J. DUDERSTADT and L. J. HAMILTON, *Nuclear Ractor Analysis*. New York, NY: John Wiley & Sons, 1976.
60. J. F. BRIESMEISTER, "Mcnp--a General Monte Carlo Code for Neutron and Photon Transport " LA-7396-M-Rev. 2, Los Alamos National Laboratory. Most recent version available from Radiation Safety Information Computational Center, Oak Ridge National Laboratory, Oak Ridge, TN, (1986).
61. R. P. RECHARD, L. C. SANCHEZ, and H. R. TRELLUE, "Consideration of Nuclear Criticality When Directly Disposing Highly Enriched Spent Nuclear Fuel in Unsaturated Tuff, Part 1: Nuclear Criticality Constraints," *Nuclear Technology,* **144**, 201 (2003).
62. H. C. PAXTON, J. T. THOMAS, D. CALLIHAN, and E. B. JOHNSON, "Critical Dimensions of Systems Containing ^{235}U, ^{239}Pu and ^{233}U," TID-7028, Los Alamos National Laboratory; Oak Ridge National Laboratory, (1964).
63. E. D. CLAYTON and W. A. REARDON, "Chapter 27: Nuclear Safety and Criticality of Plutonium," in *Plutonium Handbook: A Guide to the Technology*: American Nuclear Society, 1980.
64. H. K. CLARK, "Subcritical Limits for Uranium-235 Systems," *Nuclear Science and Engineering,* **81**, 3, 351–378 (1982), doi: 10.13182/NSE82-A20279.
65. J. K. THOMPSON, "Minimum Critical Mass of Plutonium-Polyethylene System Found to Be Significantly Lower Than Plutonium-Water System," *Nuclear Technology,* **33**, 2, 235–236 (1977).
66. G. W. NEELEY, D. L. NEWELL, S. L. LARSON, and R. J. GREEN, "Reactivity Effects of Moderator and Reflector Materials on a Finite Plutonium System," SAIC-1322-001 Rev. 1, Science Applications International Corporation, (2004).
67. T. W. LAMBE and R. V. WHITMAN, *Soil Mechanics*. New York: John Wiley & Sons, 1969.
68. W. A. DEER, R. A. HOWIE, and J. ZUSSMAN, *An Introduction to the Rock-Forming Minerals*. Longman, 1985.
69. C. LIU, Z. ZHU, F. LI, T. LIU, C. LIAO, J.-J. LEE, K. SHIH, L. TAO, and Y. WU, "Fe(Ii)-Induced Phase Transormation of Ferrihydrite: The Inhibition Effects and Stabilization of Divalent Metal Cations," *Chemical Geology,* **444**, 110–119 (2016).
70. Z. WANG, R. C. MOORE, M. J. MASON, and R. K. KUKKADAPU, "A Study of Corrosion Products of Mild Steel in High Ionic Strength Brines," *Waste Management,* **21**, 4, 335–341 (2001).
71. C. HANSEL, M., S. G. BENNER, and S. FENDORF, "Competing Fe(Ii)-Induced Mineralization Pathways of Ferrihydrite," *Envionmental Science Technology,* **39**, 18, 7147–7153 (2005).
72. F. GAUTHIER-LAFAYE, P. HOLLIGER, and P. BLANC, "Natural Fission Reactors in the Franceville Basin, Gabon: A Review of the Conditions and Results of a "Critical Event" in a Geologic System," *Geochimica et Cosmochimica Acta,* **60**, 23, 4831–4852 (1996).
73. F. GAUTHIER-LAFAYE and F. WEBER, "Natural Nuclear Fission Reactors: Time Constraints for Occurrence, and Their Relation to Uranium and Manganese Deposits and to the Evolution of the Atmosphere," *Precambrian Research,* **120**, 81–100 (2003).
74. S.-E. BENTRIDI, B. GALL, F. GAUTHIER-LAFAYE, A. SEGHOUR, and D.-E. MEDJADI, "Inception and Evolution of Oklo Natural Nuclear Reactors," *Comptes Rendus Geoscience,* **343**, 738–748 (2011).
75. L. J. GRATTON, E. GREENSPAN, P. F. PETERSON, and W. E. KASTENBERG, "Sensitivity Analysis for Autocatalytic Criticality Events in Geologic Media," *Transactions American Nuclear Society,* **78**, 168 (1998).
76. L. J. GRATTON, W. E. KASTENBERG, P. F. PETERSON, N. STONE, and J. ZIMMERMAN, "Phenomena Affecting the Dynamics of Critical Deposits in Tuff," Eighth International High-Level Radioactive Waste Management Conference, Las Vegas, NV, May 11-14, 1998, (1998).
77. L. J. GRATTON, W. E. KASTENBERG, and P. F. PETERSON, "Bounding Energy Production Estimates for Autocatalytic Fissile Material Deposits in Geologic Media," Proceedings Topical Meeting on Criticality Safety Challenges in the Next Decade, Chelan, WA, September 7-11, 1997.p. 130 (1997).
78. EPA (US ENVIRONMENTAL PROTECTION AGENCY), "40 CFR Part 194: Criteria for the Certification and Re-Certification of the Waste Isolation Pilot Plant's Compliance with the 40 Cfr Part 191 Disposal Regulations; Final Rule," *Federal Register,* **61**, 28, 5224–5245 (1996).

Information Only



Sandia National Laboratories

Sandia National Laboratories is a multimission laboratory managed and operated by National Technology & Engineering Solutions of Sandia LLC, a wholly owned subsidiary of Honeywell International Inc. for the U.S. Department of Energy's National Nuclear Security Administration under contract DE-NA0003525.

Information Only